Investigating the Dependence of the Effectiveness of Carbon Dioxide Removal on the Amount and Rate of Removal

by

Chloe Papalazarou

B.Sc., University of Guelph, 2019

Thesis Submitted in Partial Fulfillment of the
Requirements for the Degree of
Master of Science

in the
Department of Geography
Faculty of Environment

© Chloe Papalazarou 2021
SIMON FRASER UNIVERSITY
Summer 2021

Declaration of Committee

Name: **Chloe Papalazarou**

Degree: **Master of Science (Geography)**

Title: **Investigating the Dependence of the Effectiveness of Carbon Dioxide Removal on the Amount and Rate of Removal**

Committee: **Chair:**   **William Jesse Hahm**
Assistant Professor, Geography

Kirsten Zickfeld
Supervisor
Distinguished Professor, Geography

Karen Kohfeld
Committee Member
Professor, Resource and Environmental Management

Damon Matthews
Examiner
Professor and Research Chair
Climate Science and Sustainability, Geography, Planning and Environment
Concordia University

Abstract

Most future climate scenarios consistent with the 1.5-2°C limits set by the Paris Agreement include carbon dioxide removal (CDR) as an important mitigation measure. Here, we investigate the land carbon cycle response to different magnitudes and rates of CDR using an Earth System Model of Intermediate Complexity. We show that the climate and carbon cycle response 100 years after the end of the removal is dependent on the magnitude of CDR and depends slightly on the rate of CDR. Several centuries after the end of the removal the response is largely rate independent at the global scale. At the regional scale, small land carbon differences of opposite sign persist between the tropics, , and northern mid and high latitudes several centuries after the end of the removal. The results of this thesis inform how CDR scenarios can be deployed most effectively with regard to drawing down atmospheric CO_2 and mitigating warming.

Keywords: climate change; carbon cycle; negative emissions; carbon dioxide removal (CDR); climate modelling; Earth systems

To my parents, Brenda and Dan Papalazarou for their unwavering support in everything I set out to do, and to my friends, near and far (you know who you are), for bringing endless joy and inspiration into my life.

Acknowledgements

I would like to acknowledge and thank Dr. Kirsten Zickfeld for her insight, mentorship, and understanding throughout this research. I am thankful for her efforts in helping me familiarize myself in a new discipline, providing me with resources, advice, and encouragement throughout the process. This research would not have been possible without her expertise, ideas, and insight. I am thankful for her collaboration in creating a fulfilling, challenging, and supportive work environment. I also would like to acknowledge and thank Dr. Karen Kohfeld for her guidance throughout the writing process, and for her expertise and valued perspective.

In addition, I'd like to thank my fellow members of the Climate Lab for their assistance and perspective in helping me to decode confusing results, resolve model difficulties, and for providing feedback on presentations. To Alex for helping with my understanding of UVic ESCM, reviewing my writing and Python code, and for his friendship and encouragement throughout this degree.

I'd also like to thank fellow members of the Geography department for fostering a welcoming work environment, and for the friends I've made along the way.

Table of Contents

List of Tables

List of Figures

Chapter 1.　　Introduction

The 2016 Paris Agreement was a call for action to limit the detrimental effects of climate change. The agreement outlines a goal to limit global warming to well below 2°C above pre-industrial levels, with further efforts to reduce warming to 1.5°C (UNFCCC 2018). If we are to limit the impacts of anthropogenic interference on the climate system to be consistent with the IPCC's suggested 1.5°C level of warming, we have an estimated 160GtC left to emit from 2018 to have a 50% probability of reaching this target, and an estimated 110 GtC left to emit to have a 66% probability (Rogelj, Shindell, et al., 2018). Currently, we are emitting 11GtC/year into the atmosphere (Rogelj et al., 2019), which leaves 10-14 years before this target is reached (Rogelj, Shindell, et al., 2018). Even with substantial mitigation of carbon dioxide (CO_2) emissions, atmospheric CO_2 removal is required to limit anthropogenic interference with the climate system in most scenarios which limit warming to 1.5°C. All future climate scenarios which limit warming to 1.5°C without overshooting this temperature target use atmospheric CO_2 removal (Rogelj, Shindell, et al., 2018). The longer CO_2 emissions reductions are delayed, a heavier dependence on atmospheric CO_2 removal will be required to reach this 1.5°C target.

The removal of anthropogenic CO_2 by human intervention is referred to as "negative emissions", or carbon dioxide removal (CDR) (Minx et al., 2018). Negative emissions technologies (NETs) only remove CO_2 that has been released into the atmosphere, and do not refer to reductions in CO_2 emissions (Minx et al., 2018). CDR techniques include afforestation, reforestation, and soil carbon sequestration, which are well known and are widely used practices for CO_2 sequestration and climate change mitigation (Nabuurs et al., 2007, Smith et al., 2007). Other technologies such as Bioenergy with Carbon Capture and Storage (BECCS), focus on sequestration and storage through artificial means (Boucher et al., 2014).

The effects of global warming are irreversible in the absence of CDR. If all CO_2 emissions were to cease today and no CDR were implemented, surface air temperatures would remain approximately constant (Cao & Caldeira, 2010; Eby et al., 2009; Gillett et al., 2010; MacDougall et al. 2020; Mathesius et al., 2015; Matthews & Caldeira 2008).

Even 10,000 years after CO_2 emissions cease, Earth system model simulations show about 15-30% of the total CO_2 emitted remaining in the atmosphere, and a remaining 75% of the maximum surface temperature anomaly (Eby et al., 2009). Therefore, even with efforts to reduce overall emissions, we expect to require CDR to reverse the effects of climate change in our lifetime (Fuss et al., 2018; Minx et al., 2018).

There is still much we do not understand about how large-scale CO_2 removal affects the carbon cycle and climate system on century timescales. For example, the effects of removal on the carbon cycle, surface air temperature, atmospheric CO_2, and on carbon storage in the land and ocean reservoirs for various levels and rates of CDR are not well quantified. Before any large-scale implementation of CDR is launched, the effects of CO_2 removal on the Earth system must be well understood to develop effective climate change mitigation strategies which involve CDR. The goal of this research is to further investigate the effects of different magnitudes and rates of CDR on the Earth system in terms of the changes in surface air temperatures, carbon fluxes between the land and ocean reservoirs and the atmosphere, and storage in the land and ocean reservoirs, on multi-century timescales.

1.1. Background

1.1.1. Natural Climate-Carbon Cycle Dynamics

Carbon in the Earth system is partitioned into atmospheric, oceanic and terrestrial reservoirs naturally through the carbon cycle. Photosynthesis drives the uptake of CO_2 in plants, and plant respiration and decomposition of organic material in soils add CO_2 to the atmosphere (Houghton, 2013). The balance between the uptake of CO_2 through photosynthesis, and the release of CO_2 through plant respiration is known as net primary productivity (NPP). In the surface ocean, CO_2 dissolves and dissociates into the carbonate buffer system which combines CO_2 and H_2O to create carbonate, bicarbonate, and H+ ions (Houghton, 2013). This buffer system controls the dissolution of CO_2 in the ocean and is a component of the solubility pump (Houghton, 2013; Mathesius et al., 2015). Phytoplankton in the surface ocean take up dissolved CO_2 for photosynthesis, and are

food for surface marine life (Houghton, 2013). When marine life excretes waste products into the surface ocean, these waste products contain carbon and other nutrients, which sink to depth and decompose in the water column or settle to the sea floor (Houghton, 2013). This process of cycling carbon into the deep ocean is referred to as the biological pump. Deep water formation in the ocean is the process of cold, dense water in the high latitude regions sinking to the deep ocean, carrying carbon from the surface ocean into the deep ocean (Stocker & Wright, 1991). Deep water formation facilitates the movement of water from the surface to the deeper ocean, which drives the solubility pump. Upwelling in regions of divergent winds bring nutrients back to the ocean's surface and is a component of the biological pump.

1.1.2. Carbon Cycle Response to Positive CO_2 Emissions

Over the past decade, the land and ocean have acted as a sink of CO_2 from the atmosphere, taking up about 54% of the carbon that has been released into the atmosphere. On land, photosynthesis occurs at a faster rate than soil respiration, with the land taking up 3.1 GtC/year (Friedlingstein et al., 2020). Elevated CO_2 concentrations drive photosynthesis by increasing the stomatal conductance of CO_2 into plant tissue, which allows for more efficient gas exchange and water retention (Leakey et al., 2009). This increases uptake as a result of CO_2 saturation in the atmosphere by up to 40%, and the resulting increased rate of photosynthesis is called the CO_2 fertilization effect (Leakey et al., 2009). The ocean is also currently a carbon sink because there is a greater concentration of CO_2 in the atmosphere than in the surface ocean which "pushes" CO_2 into the ocean via this partial pressure gradient at a rate of 2.6 GtC/year (Friedlingstein et al., 2020).

Because of competing climate-carbon cycle feedbacks is it unlikely the land and ocean carbon sinks will continue to take up this fraction of CO_2 in the future (Friedlingstein et al., 2020). Increasing CO_2 in the atmosphere will increase the rate of uptake by the sinks initially. On land, the increasing temperature as a result of this rise in CO_2 will cause water stress in plants reducing the vegetation available for photosynthetic uptake of CO_2, and cause increased decomposition in soils, releasing CO_2 back into the

atmosphere (Cox et al., 2000; Raich et al., 2013). Many low latitude regions are projected to experience a loss of vegetation due to increased temperatures (Cox et al., 2000; Friedlingstein et al., 2020; Raich et al., 2013), which may lower the carbon storage capacity of the terrestrial biosphere from increasing soil respiration rates, and decreasing vegetation cover due to decreased water availability and NPP (Bastos et al., 2018; Cox et al., 2000; Friedlingstein et al., 2020; Raich et al., 2013). This same warming causes an increase in vegetation cover in high latitude regions due to increased NPP and earlier onset of growing seasons (Bastos et al., 2018; Cox et al., 2000). The potential carbon released from melting permafrost is estimated to be 3.1GtC per °C warming over the 21st century, which could have large implications for the Earth system also, but permafrost feedbacks are not well understood and require further investigation (Schuur et al., 2015; Turetsky et al., 2020). In the oceans, increasing surface ocean temperatures decreases the ability for CO_2 to dissolve in seawater, leaving a higher fraction remaining in the atmosphere (Mathesius et al., 2015). High temperatures also reduce ocean circulation by causing thermal stratification of the ocean (Mathesius et al., 2015). This affects the process of formation of colder, denser, CO_2 rich waters sinking into the deep ocean, especially in the North Atlantic regions (Mathesius et al., 2015). In the cryosphere, temperature increases are causing sea ice to melt, which further freshens high latitude waters. Freshening of seawater decreases its density, making it less susceptible to sink to the deep ocean (Stocker and Wright 1991). Thermal stratification and freshening of seawater weaken ocean circulation, reducing ocean uptake of CO_2 from the atmosphere (Mathesius et al., 2015; Stocker and Wright 1991).

1.1.3. Carbon Cycle Response to Negative CO_2 Emissions

Some simulations that study the effects of CDR on the carbon cycle and climate look at scenarios in which a fraction or all (50-500 GtC) of anthropogenic CO_2 is instantaneously removed from the atmosphere (Cao & Caldeira, 2010; Vichi et al., 2013; Zickfeld et al., 2021). Although the amount and method of CO_2 removal depicted in these scenarios is idealized, they serve as a baseline to help us understand the potential changes to major variables in the Earth system. In studies in which all, or a large fraction of anthropogenic CO_2 emissions are removed from the atmosphere, an immediate release of

CO₂ from the land and ocean reservoirs occurs (Cao & Caldeira, 2010; Vichi et al., 2013; Zickfeld et al., 2021). The magnitude of the release depends on the amount of CO_2 removed and is a result of the reversal of the partial pressure gradient between the atmosphere and the surface ocean and the faster reduction in NPP than soil respiration that causes soil respiration to dominate on land (Cao & Caldeira, 2010; Vichi et al., 2013; Zickfeld et al., 2021). After a removal of all anthropogenic CO_2 (500 GtC), the ocean initially returns CO_2 to the atmosphere, and becomes a sink of CO_2 25 years after removal takes place despite the reduction in atmospheric CO_2 concentration due to the slow response of the deep ocean, which is still responding to elevated CO_2 concentrations prior to CDR (Vichi et al., 2013). On land, plants respond to a decline in atmospheric CO_2 due to CO_2 removal by taking up less CO_2, and NPP occurs at a slower rate. The rate of respiration in soils does not initially decline as much as the rate of photosynthesis when CO_2 is removed from the atmosphere. Respiration is controlled by changes in surface temperature (Cao & Caldeira, 2010; Houghton, 2013; Raich et al., 2013). Since temperature change lags changes in atmospheric CO_2 concentration by years to decades, the response of changes in the rate of respiration lags the changes in atmospheric CO_2 concentration (Cao & Caldeira, 2010; Zickfeld et al., 2021). Following a removal of all anthropogenic CO_2 from the atmosphere, the rate of respiration decreased by less than half of the rate of photosynthesis immediately following removal (Cao & Caldeira, 2010).

The climate-carbon cycle response to CO_2 removal depends on whether CDR is applied from a state of the Earth system at equilibrium with a given radiative forcing, or a state where the system is still adjusting to the forcing ("transient" state) (Jones et al., 2016; Zickfeld et al., 2021). In studies that simulate different rates of atmospheric CO_2 removal following a trajectory of positive CO_2 emissions, the ocean and land sinks weaken considerably in response to increased CDR (Jones et al., 2016; Tokarska & Zickfeld, 2015). The reduction of the partial pressure gradient between the atmosphere and the surface ocean reduces ocean uptake, weakening the ocean sink as atmospheric CO_2 decreases (Jones et al., 2016). Due to the long-time scale it takes for the deep ocean to equilibrate with changes in atmospheric CO_2, the ocean continues to take up CO_2 for centuries after emissions become negative (Jones et al., 2016; Mathesius et al., 2015). On land, the reduction of atmospheric CO_2 under a constant rate of CDR causes the reduction

in the rate of NPP, weakening the land sink (Jones et al., 2016; Tokarska & Zickfeld, 2015). Three out of four Earth System Models (ESMs) in the study by Jones et al. simulate the land turning into a source of CO_2 after decades of constant CDR (Jones et al., 2016). The decadal-scale lag in response to CDR occurs due to vegetation shifts in the northern latitudes which are continuously responding to elevated temperatures from previous positive emissions (Tokarska & Zickfeld, 2015). Higher temperatures allow vegetation to grow at higher northern latitudes, thus increasing the initial land sink despite emissions being net negative (Tokarska & Zickfeld, 2015). Due to the inertia of the climate system, temperature is influenced by previous positive emissions on centennial timescales, causing a nonlinear response to CDR from a transient state (Zickfeld et al., 2021, 2016). In model simulations where CO_2 removal takes place from an Earth system in equilibrium, the temperature response to CO_2 removal becomes linear (Zickfeld et al., 2021, 2016).

Studies find that the centennial-scale carbon cycle response is independent of the rate of CO_2 removal and depends only on the total amount of removal (Jones et al., 2016; Tokarska & Zickfeld, 2015, Zickfeld et al., 2021). In simulations where the same cumulative amount of CO_2 is removed from the atmosphere at different rates, the century-scale Earth system response is shown to be path independent (Jones et al., 2016; Zickfeld et al., 2021). However, these studies do not perform a systematic investigation of the dependence of Earth system response on the rate of CDR. When quantifying the Earth system response to CO_2 removal based on the cumulative amount of removal, the airborne fraction (AF) (defined in Table 1) depends on the magnitude of removal, while the perturbation airborne fraction (PAF) (Table 1) is only slightly dependent on the magnitude of removal on century timescales (Jones et al., 2016; Tokarska & Zickfeld, 2015).

The atmospheric CO_2 concentration and associated state of the Earth system from which CDR is applied has an impact on the centennial-scale carbon cycle response to CDR (Jones et al., 2016; Zickfeld et al., 2021). In simulations in which 320 GtC are removed from different RCP scenarios, the resulting reduction in atmospheric CO_2 varies widely with the scenario (Jones et al., 2016). For RCP8.5, a high emissions scenario,

atmospheric CO_2 decreases by 274 GtC, while for RCP2.6, the same 320GtC removal only leads to a decrease of 178 GtC (Jones et al., 2016). In simulations in which 100 GtC is removed from an Earth system in equilibrium with the pre-industrial or4 times the pre-industrial CO_2 concentration, atmospheric CO_2 decreases by 27 GtC and 76 GtC, respectively (Zickfeld et al., 2021). At higher initial CO_2 concentrations, the release of CO_2 from the land and ocean in response to CDR is reduced compared to CDR from lower initial CO_2 concentrations. This is due to the non-linear dependence of the CO_2 fertilization effect on land, which results in less of a decline in NPP and vegetation carbon for CDR from a higher background CO_2 concentration (Zickfeld et al., 2021). In the ocean, the non-linear dependence of the buffer capacity on the pCO2 gradient results in less of a release of CO_2 from the ocean for removals from a higher background concentration (Zickfeld et al., 2021). Additionally, thermal stratification of the ocean at higher background CO_2 concentrations prevents upward mixing of carbon rich waters in the deep ocean, resulting in less of a release of carbon from the ocean (Zickfeld et al., 2021).

1.1.4. Effectiveness of CDR

Effectiveness refers to the ability of CDR to reduce the carbon burden in the atmosphere or surface warming for a given amount of CO_2 removal. It can be defined in several ways (Table 1). A metric that has been proposed to measure the effectiveness of CDR is the cumulative airborne fraction (CAF). For positive emissions, the CAF is a dimensionless quantity commonly defined as the ratio of the rise in atmospheric CO_2 burden to cumulative CO_2 emissions. Equivalently, for CDR, the CAF can be defined as the ratio of the drop in atmospheric CO_2 burden to cumulative CO_2 emissions (Jones et al., 2016; Tokarska & Zickfeld, 2015). When defined in this way, the effectiveness of CDR increases as the CAF increases (Tokarska & Zickfeld, 2015). A second commonly used metric to quantify the change in atmospheric CO_2 under positive CO_2 emissions is the instantaneous airborne fraction (AF), defined as the ratio of the rise in atmospheric CO_2 to the CO_2 emissions over a single year (Jones et al., 2016). However, when considering scenarios in which net CO_2 emissions change in sign, these metrics are not always well defined and may present results which are difficult to interpret (Jones et al.,

2016). When comparing emissions scenarios, if it is desired to calculate the effect of removing additional carbon, the AF or CAF are not useful metrics to determine the difference additional CDR can make. A third measure, the perturbation airborne fraction (PAF), is defined as the change in atmospheric CO_2 from the additional carbon removed from a reference emissions scenario (equation in Table 1), and is useful when needing to compare the effectiveness of additional amounts of CDR in an existing scenario (Jones et al., 2016). Once a PAF is calculated for a given scenario, it can be approximately applied to other removals within the same scenario to estimate their potential effectiveness (Jones et al., 2016).

The effectiveness of CDR can also be defined through its effects on temperature. The surface air temperature change for a given amount of positive CO_2 emissions is known as the transient climate response to cumulative CO_2 emissions (TCRE) (Matthews et al., 2009). The TCRE can be adapted to define the effectiveness of a given amount of CDR in reducing surface air temperatures by taking the change in temperature over the cumulative CO_2 removed (equation in Table 1); this measure is referred to as the transient climate response to removals (TCRR) (Zickfeld et al., 2021).

Table 1:   Summary of the different measures used to determine effectiveness of a given amount of CDR

Measure of Effectiveness	Definition	Equation
Airborne Fraction (AF)	Change in atmospheric CO_2 burden per year (GtC/y) over the CO_2 emissions or removals (E) per year (GtC/y)	$\dfrac{\Delta CO_2}{E}$
Cumulative AF (CAF)	Change in atmospheric CO_2 burden over a given period (GtC) over the cumulative CO_2 emissions or removals (CE; GtC) for that period	$\dfrac{\Delta CO_2}{CE}$
Perturbation AF (PAF)	The change in atmospheric CO_2 burden (GtC) relative to a reference scenario without CDR over the cumulative CO_2 removed (CR)	$\dfrac{\Delta CO_2 - \Delta CO_{2(ref)}}{CR}$
Transient Climate Response to Removals (TCRR)	The change in surface air temperature (°C) over a given period over the cumulative CO_2 removals (CE; GtC) over that period	$\dfrac{\Delta T}{CE}$

Carbon cycle responses to CDR remain under investigated in current research. How the global Earth system response is impacted by different rates and magnitudes of CDR on policy relevant 100-year timescales is not well understood. The changes to the flux and storage of carbon between the atmosphere, ocean, and land reservoirs for different rates and magnitudes of removal will determine the global Earth system response to CDR. Additionally, the effectiveness of CDR at reducing the mass of atmospheric CO_2, and surface air temperature within our lifetime is poorly quantified in current research. Lastly, the spatial land carbon response to different magnitudes and rates of CDR has not been investigated in past research. It is important to understand how the Earth system responds to CDR spatially on land to identify any highly impacted areas in terms of changes to carbon storage and productivity, as some NETs rely heavily on the land system for carbon sequestration.

Chapter 2.　　Research Questions

Research to date lacks a complete understanding of the long-term global and regional carbon cycle response to removal of CO_2 at different rates. First, some studies show an extreme case scenario of a large, instantaneous removal of a large fraction, or all anthropogenic CO_2 (Cao & Caldeira, 2010; Held et al., 2010; Vichi et al., 2013). However, more realistic scenarios, such as lower rates of annual CO_2 removal over decades, are less studied. The timelines of these more plausible scenarios will more likely inform policy and the extent of climate change in the future. Second, the effectiveness of CDR at different magnitudes and rates remains poorly understood. The effectiveness of CDR and its dependence on the magnitude of removal must be known to develop useful climate change mitigation strategies which involve CDR. Third, the response of the terrestrial carbon cycle to different rates and magnitudes of CDR is especially understudied. The spatial land response and its dependence on the amounts and rates at which CDR is deployed has not been investigated. The land and ocean are the largest carbon sinks on Earth, and understanding their responses to declining CO_2 concentrations is necessary to effectively implement climate change solutions. The following research questions aim to investigate the Earth system response to CDR through a systematic analysis of (a) differences in the continental-to-global climate-carbon cycle responses on centennial timescales, depending on the amount or rate of CO_2 removal, and (b) the effectiveness of CDR in reducing atmospheric CO_2 concentrations and surface air temperature for each scenario, with a focus on the land. The research questions include:

1. To what extent is the climate-carbon cycle response to removal dependent on the amount or rate of CO_2 removal?

2. To what extent is the effectiveness of CDR dependent on the amount or rate of CO_2 removal?

3. What is the spatial climate-carbon cycle response to CDR on land?

I use an Earth System Modelling approach to answer these research questions. I perform 1000-year simulations to encompass the centennial response of the Earth System to CDR. The spatial capacity of ESMs to describe the carbon-climate response at a

regional scale, in addition to their ability to project changes over century timescales provides the approach required to successfully answer these research questions.

Chapter 3.   Methodology

3.1. UVic ESCM Model Description

The University of Victoria Earth System Climate Model (UVic ESCM) is an Earth Systems Model of Intermediate Complexity (EMIC), that is, a fully coupled climate-carbon cycle model used to assess the long-term (decadal to millennial timescale) effects of anthropogenic CO_2 emissions on the Earth system (Eby et al., 2009, Mengis et al., 2020). The UVic ESCM consists of a 2D energy moisture balance model of the atmosphere coupled to a 3D ocean general circulation model, a land surface model, a dynamic vegetation model, and terrestrial and oceanic carbon cycle models (Eby et al., 2009; Mengis et al., 2020; Weaver et al., 2001). The ocean and atmospheric models additionally interact with a dynamic/thermodynamic sea ice model (Bitz et al., 2001; Weaver et al., 2001). The model covers a global distribution with a grid cell resolution of 3.6° latitude by 1.8° longitude, which allows continental-scale detail to be resolved (Weaver et al., 2001). Figure 1 is a schematic of the UVic ESCM which outlines how each component within the model interacts through the exchange of energy, carbon, and water.
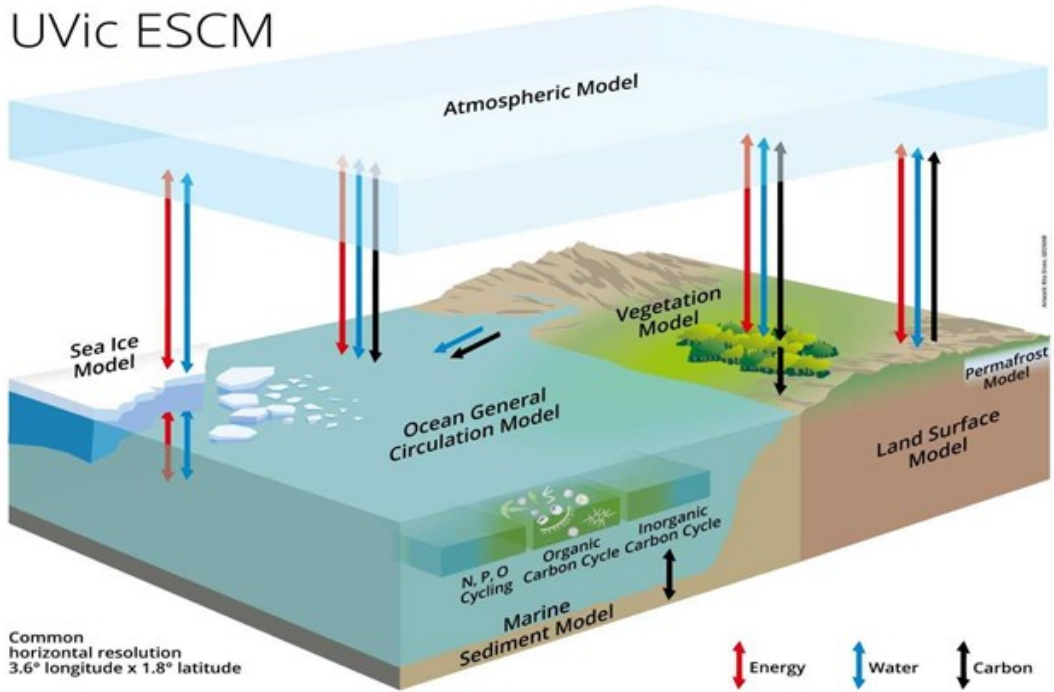
Figure 1:   Schematic representation of the UVic ESCM and each of its components and how they are connected through fluxes of energy, carbon, and water (Mengis et al. 2020). Figure reproduced with permission from Mengis et al., (2020).

3.1.1. Atmospheric Component

The formulation of the atmospheric component of the UVic ESCM is based on energy and moisture balance equations (Weaver et al., 2001). The energy balance in the atmosphere is determined by the balance of incoming and outgoing solar radiation at the top of the atmosphere, and the fluxes of latent heat, sensible heat, and longwave radiation from the surface (Weaver et al., 2001). The vertically-integrated atmospheric energy balance is described by equation 1:

$$\rho_{SA} h_T C_{pa} \frac{\partial T_{SA}}{\partial t} = Q_T + Q_{SW} C_A + Q_{LW} + Q_{LH} + Q_{SH} - Q_{PLW} \tag{1}$$

Where Q_T represents the heat transport term, which parameterizes the diffusion of heat in the atmosphere, Q_{SW} is the incoming shortwave radiation at the top of the

13

atmosphere, Q_{LW} is the longwave radiative flux into the atmosphere, Q_{LH} is the latent heat flux into the atmosphere, Q_{SH} is the sensible heat flux, Q_{PLW} is the outgoing planetary longwave radiation which defines the radiative forcing associated with changes in atmospheric CO_2 concentration, C_A is the atmospheric absorption coefficient which depends on absorption by water vapour, ozone, dust, and clouds, $\rho_{SA} h_T C_{pa} \frac{\partial T_{SA}}{\partial t}$ is the heat storage at sea level, ρ_{SA} is the surface air density, h_T is the constant scale height for temperatures and C_{pa} is the specific heat of air at constant pressure (Weaver et al., 2001).

The moisture balance within the atmosphere is determined by the specific humidity based on the balance between evaporation and precipitation at the surface, and is described by equation 2:

$$\rho_{SA} h_q \left\{ \frac{\partial q_{SA}}{\partial t} - \nabla \cdot (\kappa \nabla q_{SA}) \right\} = p_0 (E - P) \tag{2}$$

Where E is evaporation (m s^{-1}), P is precipitation (m s^{-1}), $\rho_{SA} h_q \frac{\partial q_{SA}}{\partial t}$ is the moisture storage in the atmosphere, and the divergence term ∇ defines the moisture transport in and out of a model grid cell. h_q is the constant scale height for specific humidity, κ is an eddy diffusivity, which depends on latitude, and p_0 is the density of water (Weaver et al., 2001).

Heat and moisture from the surface are distributed through the atmosphere by diffusion and advection by winds (Weaver et al., 2001). The decrease in heat energy as one moves vertically through the atmosphere is the lapse rate defined by the surface air temperature, the specific humidity, and the outgoing longwave radiation from Earths surface (Weaver et al., 2001). The lapse rate is globally averaged within the model. Winds within the model are prescribed, and dynamical wind feedbacks determined by latitudinally varying latent and sensible heat fluxes, and surface air temperature gradients are represented (Weaver et al., 2001). Precipitation in the model is determined by the relative humidity at the surface and is assumed to occur when the relative humidity (r) is greater than a threshold value of 0.85 (Weaver et al., 2001). A threshold surface air

temperature of roughly -5°C determines if the precipitation will fall as rain or accumulate as snow (Weaver et al., 2001).

3.1.2. Ocean Component

The oceanic component of the model is based on the Geophysical Fluid Dynamics Laboratory (GFDL) Modular Ocean Model (MOM) version 2.2 (Pacanowski, 1995). The ocean model contains 19 vertical levels (Weaver et al., 2001). It is a general circulation model (GCM), which means it solves fundamental equations in terms of conservation of mass, momentum, energy, and equations of state in order to determine the specific conditions of each vertical layer (McGuffie and Henderson-Sellers, 2014). The ocean model is 3 dimensional, with 19 vertical layers, , transports heat, carbon, and salt vertically and horizontally (Weaver et al., 2001). Mixing in the ocean is represented by a scheme of diapycnal mixing induced by tides over rough topography (Mengis et al., 2020). The model represents density as a function of temperature, salinity, and pressure (Pacanowski, 1995). Surface winds affect pressure and mixing in the surface layer of the ocean model (Weaver et al., 2001).

The ocean model represents organic and inorganic carbon cycles (Mengis et al., 2020). The concentration of DIC in the surface ocean is determined through changes in precipitation, evaporation, and runoff, and the air-sea gas exchange flux which is based on the partial pressures of CO_2 in the atmosphere and ocean surface layer (Keller et al., 2012). Dissolved inorganic carbon (DIC) within the model is transported to the deep ocean through mixing and ocean circulation. In addition to DIC, alkalinity ($CaCO_3$) is included as a biogeochemical tracer (Keller et al., 2012). Also embedded within the ocean circulation model are two phytoplankton classes, zooplankton, nitrate (NO_3), phosphate (PO_4), oxygen (O_2), and particulate detritus (Keller et al., 2012). Equations in the biogeochemical components of the ocean model describe phytoplankton growth which is limited by light and iron, and zooplankton growth and grazing (Mengis et al., 2020).

3.1.3. Sea Ice Component

The dynamic/thermodynamic sea ice model in the UVic ESCM represents sea ice processes, ice surface temperature, ice thickness and area. Thermodynamic processes in the model influence the extent of the sea ice, while dynamic processes regulate the thickness and concentration (Weaver et al., 2001). Snow accumulation on sea ice depends on the surface energy balance, and the albedo of the snow is dependent on its accumulation depth, and surface air temperature in relation to the snow's critical temperature (Weaver et al., 2001).

3.1.4. Land Surface and Vegetation

The land surface model within the UVic ESCM is adapted from the Hadley Centre's Met Office Surface Exchange Scheme (MOSES), coupled to the Top-down Representation of Interactive Foliage and Flora Including Dynamics (TRIFFID) dynamic global vegetation model (Meissner et al., 2003). The top 8 layers of MOSES extend to 10m in depth and represent soil (Mengis et al., 2020). Heat, water, and carbon exchange occurs with the top 6 layers of soil up to a depth of 3.35m (Eby et al., 2009; Mengis et al., 2020). Organic carbon in the top layer is received from litterfall from the dynamic global vegetation model and distributed to the rest of the 6 layers as a decreasing function of depth (Mengis et al., 2020). Land carbon fluxes are calculated within MOSES and are allocated to vegetation and soil carbon pools (Matthews et al., 2004). Permafrost is also represented in the land model.

The state of the terrestrial biosphere defined in TRIFFID is determined by the soil carbon from the land surface model in combination with the structure and coverage for 5 plant function types (Meissner et al., 2003). The PFTs are broadleaf, needleleaf, shrubs, C3 grass and C4 grass (Cox, 2001). Each PFT is described by a carbon density and fractional coverage and is updated based on the carbon balance within that PFT. Carbon balance on land is based on the balance of net primary productivity in plants and respiration by plants and soils (Cox, 2001). Carbon is taken up from the atmosphere by photosynthesis in plants, litterfall from vegetation transfers carbon to the soil carbon reservoir, and respiration releases CO_2 back to the atmosphere. Vegetation carbon is

determined by the difference between carbon gained through photosynthesis and lost through litterfall. Soil carbon is determined by the balance between carbon gained by litterfall and lost through respiration (Cox, 2001). Net primary productivity in the model is determined by atmospheric CO_2 concentration and climate, and respiration in the model is determined by soil temperature, moisture, and carbon content (Cox, 2001).

3.2. Experimental Design

The CDR scenarios used in this study are designed based on maximum feasible removal rates in the literature (Fuss et al., 2018; Rogelj et al., 2018), and cumulative negative emissions from Shared Socioeconomic Pathway (SSP) scenarios which utilize plausible amounts of CO_2 removal that can be achieved with the projected advance of negative emissions technologies (NETs). SSP's are emissions trajectories which describe the potential futures of socio-economic development, technology, and energy system changes (Riahi et al., 2017). The SSP pathways that use CDR are SSP1-1.9, SSP1-2.6, SSP4-3.4, and SSP5-3.4-OS (Fuss et al., 2018). These SSPs extend to the year 2100 and have cumulative net negative emissions that range from 30 GtC to 130 GtC (SSP Public Database Version 2.0). Extension of these SSPs to the year 2300 expands the range of cumulative net negative emissions to 430 GtC (Meinshausen et al., 2020; Zickfeld et al., 2021). Total net negative CO_2 emissions in SSPs are different than the total CDR in those scenarios. Net CO_2 emissions in a given year may be positive even if CDR is deployed and will only turn negative when the amount of CDR deployed is greater than the amount of positive CO_2 emissions.
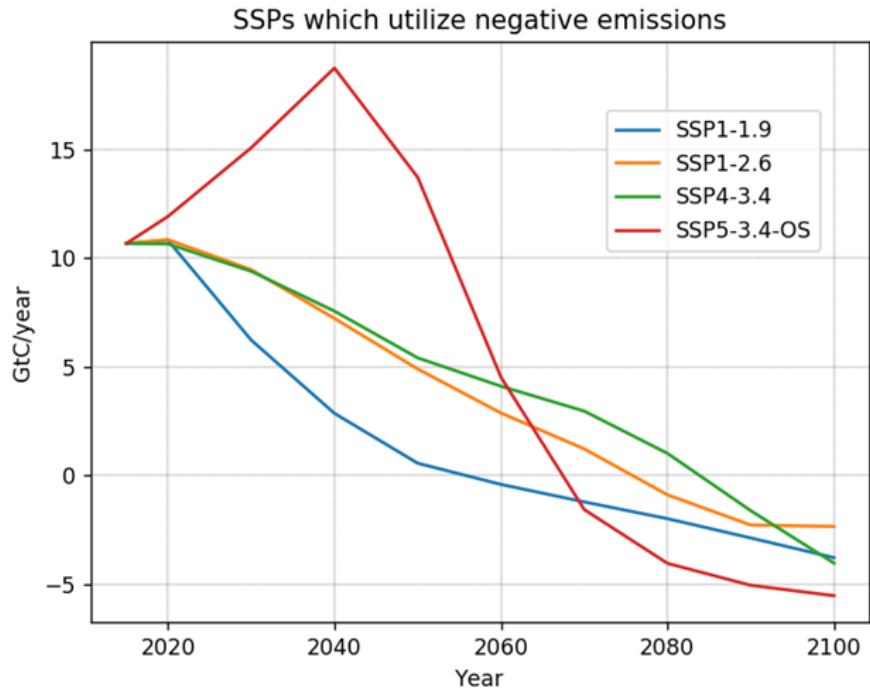
Figure 2: CO_2 emissions (GtC/year) versus time (years) for SSPs which utilize negative emissions.

Fuss et al. (2018) investigated CDR potentials in scenarios consistent with 1.5°C warming targets. They state that scenarios consistent with 1.5°C warming have a range of cumulative CDR from 40 to 320 GtC by the end of the 21st century (Fuss et al., 2018; Rogelj, Popp, et al., 2018). Current developments of NETs, suggest that, when combined, they could potentially sequester up to 7 GtC/year by 2100 (Fuss et al., 2018; Rogelj, Popp, et al., 2018).

3.2.1. Scenarios with Different Magnitudes of CDR

To investigate the magnitude dependence of the global climate-carbon response to CO_2 removal from the atmosphere, we use a set of scenarios involving different amounts of removal. Cumulative CDR amounts of 100 GtC, 200 GtC, and 500 GtC are used (Table 2). The range of cumulative CDR implemented in these simulations is informed by the approximate total net negative CO_2 emissions in SSPs that utilize negative emissions, and results from the review of negative emissions scenarios by Fuss et al., 2018. Net negative emissions are used as a proxy for CDR in this instance due to the lack

18

of information in the literature on cumulative amounts of CDR deployment for specific SSPs. To account for the CDR that is deployed during periods of net positive emissions, a broader CDR range is assumed than is reflected by the total net negative emissions deployed in each SSP. The SSP scenarios used only extend to the year 2300. Fuss et al. (2018) addresses the CDR that is deployed during periods of net positive emissions in these SSPs, but their study only extends to the year 2100. Additionally, the SSP scenarios do not exploit the full range of available CDR options (Riahi et al., 2017). Therefore, a larger range of CDR values than is provided by SSPs, Fuss et al. (2018), and Zickfeld et al. (2021) is assumed to account for CDR during periods of net positive emissions, and deployment of NETs after 2300.

3.2.2. Scenarios with Different Rates of CDR

To investigate the rate dependence of the future global climate-carbon response to CO_2 removal from the atmosphere, a set of 5 simulations is performed for each amount of removal. In these simulations, 1, 2, 5, and 10 GtC are removed per year, until the cumulative removal for each scenario group is reached (To investigate the magnitude dependence of the global climate-carbon response to CO2 removal from the atmosphere, we use a set of scenarios involving different amounts of removal. Cumulative CDR amounts of 100 GtC, 200 GtC, and 500 GtC are used (Table 2). The range of cumulative CDR implemented in these simulations is informed by the approximate total net negative CO2 emissions in SSPs that utilize negative emissions, and results from the review of negative emissions scenarios by Fuss et al., 2018. Net negative emissions are used as a proxy for CDR in this instance due to the lack of information in the literature on cumulative amounts of CDR deployment for specific SSPs. To account for the CDR that is deployed during periods of net positive emissions, a broader CDR range is assumed than is reflected by the total net negative emissions deployed in each SSP. The SSP scenarios used only extend to the year 2300. Fuss et al. (2018) addresses the CDR that is deployed during periods of net positive emissions in these SSPs, but their study only extends to the year 2100. Additionally, the SSP scenarios do not exploit the full range of available CDR options (Riahi et al., 2017). Therefore, a larger range of CDR values than

is provided by SSPs, Fuss et al. (2018), and Zickfeld et al. (2021) is assumed to account for CDR during periods of net positive emissions, and deployment of NETs after 2300.

). Rates of CDR are informed by the potentials of various NETs estimated in 2100 stated by Fuss et al., (2018) and Rogelj et al., (2018). The 10 GtC/year rate is higher than the carbon sequestration potential of 7 GtC/year stated in these reviews to represent an extreme case in this study. CDR occurs over different time periods depending on the cumulative amount of removal to be reached and the rate of removal.

Table 2:   CDR scenarios used in this study: The second and third columns identify the cumulative magnitudes that will be removed, and the rates of removal for each magnitude. All rates of removal begin at year 0 of the simulation.

	Magnitude of Removal (GtC)	Rate of Removal
Scenario group 1 (neg100)	100	Instantaneous 10 GtC/year for 10 years 5 GtC/year for 20 years 2 GtC/year for 50 years 1 GtC/year for 100 years
Scenario group 2 (neg200)	200	Instantaneous 10 GtC/year for 20 years 5 GtC/year for 40 years 2 GtC/year for 100 years 1 GtC/year for 200 years
Scenario group 3 (neg500)	500	Instantaneous 10 GtC/year for 50 years 5 GtC/year for 100 years 2 GtC/year for 250 years 1 GtC/year for 500 years

3.2.3. Model Experiments

CO_2 removal scenarios are applied from a model state at equilibrium with twice the pre-industrial CO_2 concentration (567 ppm). Prior to any CDR, the model is spun up at a constant atmospheric CO_2 concentration of 567 ppm for over 10,000 years to ensure an equilibrium state is reached. The model is spun up without the influence of anthropogenic land use change, and is referred to as a 'natural' spin up. Forcings from non CO_2 greenhouse gases and aerosols are held constant at pre-industrial values. Solar forcings are held constant at their pre-industrial values and volcanic forcing is assumed to be zero on average.

CO_2 is removed from a state of equilibrium because, due to the inertia of the climate system, removal from a transient state (i.e., a trajectory of positive CO_2 emissions) would reveal the climate-carbon response to positive emissions prior to the removal, and the climate-carbon response to the removal combined. Removal from an Earth system in equilibrium isolates the climate-carbon response to CDR from the response to the prior emissions trajectory. An atmospheric concentration at twice the

preindustrial CO_2 concentration is chosen to ensure there is enough CO_2 in the atmosphere to support experiments involving large amounts of removal (500 GtC).

CDR simulations are forced only with CO_2 (Table 2). All other natural and anthropogenic forcings are held constant at year 1850 levels for the duration of the simulations to isolate the climate-carbon cycle response to CO_2 removal.

Once the total amount of removal is reached, CO_2 emissions are set to zero and the climate system is left to evolve for up to 1000 years to ensure the long-term climate-carbon cycle responses to CDR are revealed.

In the spin up and in CDR simulations CO_2 fertilization scaling was applied and specified to 0.7, scaling down the CO_2 that plants see by 30%. Additionally, the wind field was held fixed at the pre-industrial configuration and did not respond to changes in temperature gradients

3.2.4. Effectiveness of CDR

The quantification of the effectiveness of CO_2 emissions at changing surface air temperature (TCE), and changing the mass of carbon in the atmosphere (CAF) are defined in Table 1. Here we define the CAF exclusively for negative emissions and refer to it as the cumulative removal fraction (CRF) to define the effectiveness of a given removal at reducing the carbon burden in the atmosphere. The CRF is chosen as the effectiveness metric in this study over the PAF as the PAF reduces to the CRF when using an equilibrium initial state as the reference scenario, because $\Delta CO_{2(ref)}$ is zero. The temperature change effectiveness (TCE) is defined exclusively for negative emissions and is referred to as the cooling effectiveness (CE_T) in this study to define the surface air temperature change as a fraction of the total amount of CO_2 removed. The CRF and CE_T are used to quantify the dependence of the carbon cycle and surface air temperature response on different levels and rates of CO_2 removal. The CRF and CE_T are measured 100 years after all CDR has taken place, and further quantified 500 years after all CDR has taken place.

3.2.5. Spatial Land Climate-Carbon Response to CDR

To investigate the regional land climate-carbon cycle response to CDR the spatial changes in land carbon, vegetation carbon, NPP, vegetation litter flux, changes in plant functional type (PFT) and respiration 100 years after the completion of CDR are analyzed in the experiments described in the previous section. The spatial analysis is used to identify potential mechanisms to explain differences between model experiments with varying amounts and rates of removal revealed in the global mean responses on land.

Chapter 4.   Results

4.1.   Dependence of the Climate-Carbon Cycle Response on the Amount of Removal

This section investigates the dependence of the climate-carbon cycle response to the amount of removal. A global analysis is presented which investigates the differences in the atmosphere, land, and ocean reservoir changes in response to the instantaneous removal rate for each of the three total removal amounts. Differences in the global response to removal are investigated spatially to determine the mechanisms driving the response of the Earth System at different removal amounts.

4.1.1.   Global Climate-Carbon Cycle Response

This section presents a comparison of the Earth system response to the scenarios with instantaneous removal rates for each of the three cumulative removal amounts (100 GtC, 200 GtC, 500 GtC).
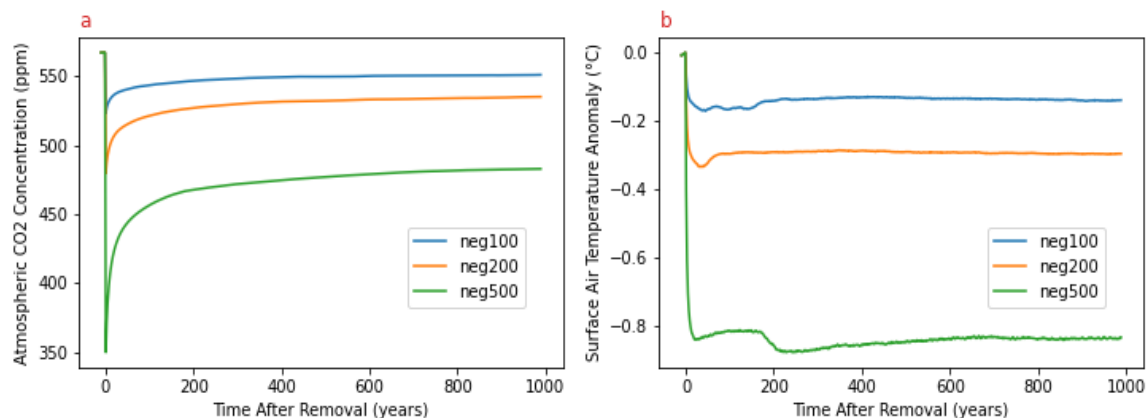
Figure 3:   Atmospheric CO_2 concentration (a) and the surface air temperature anomaly (°C) (b) vs time after removal for CO_2 removals of 100 GtC (blue), 200 GtC (orange), and 500 GtC (green) from the atmosphere. Anomalies are calculated with respect to one year before the removal takes place.

The atmospheric CO_2 concentration immediately declines in response to CDR, reaching its lowest level one year after the removal for each removal amount.

Atmospheric CO_2 does not achieve a decline of the entire amount removed, every removal amount reaches about 93% of the cumulative removal at its lowest level, with release of carbon from the land and ocean counteracting 8% of the removal in the first year. After reaching its minimum, the atmospheric CO_2 concentration rebounds, gaining CO_2 as the ocean and land release CO_2 in response to the removal. The peak cooling anomaly (Figure 3b) for each removal occurs at different times after the removal due to different temperature trajectories. The neg100 and neg200 scenarios reach their peak cooling anomalies at 45 years and 39 years after the removal, respectively. The timing of the peak cooling anomalies shows the lag in the temperature response to negative emissions. The neg500 scenario shows a different cooling trajectory than the neg100 and neg200 scenarios: following removal in the neg500 scenario, temperature immediately declines, then increases slightly for about 200 years before abruptly experiencing a second cooling of about -0.06°C after which the temperature trajectory again increases slightly. The abrupt temperature increase is due to increased ice area in the Southern Ocean, as will be discussed in detail in section 4.1.2.1. The lag in surface air temperature response to CO_2 removal is mainly controlled by the large thermal inertia of the ocean, which takes decades-centuries to respond to the decline in atmospheric CO_2 (Mathesius et al., 2015). The temperature response remains approximately stable despite atmospheric CO_2 concentrations declining and recovering due to the increase in CO_2 radiative forcing relative to the minimum atmospheric CO_2 concentration, which has a warming effect on surface air temperature, and the lagged release of heat from the ocean due to the oceans large thermal inertia has a cooling effect (Eby et al., 2009). Together, these two effects compensate each other to approximately stabilize surface air temperature at a lower level after a decline in atmospheric CO_2 concentrations.
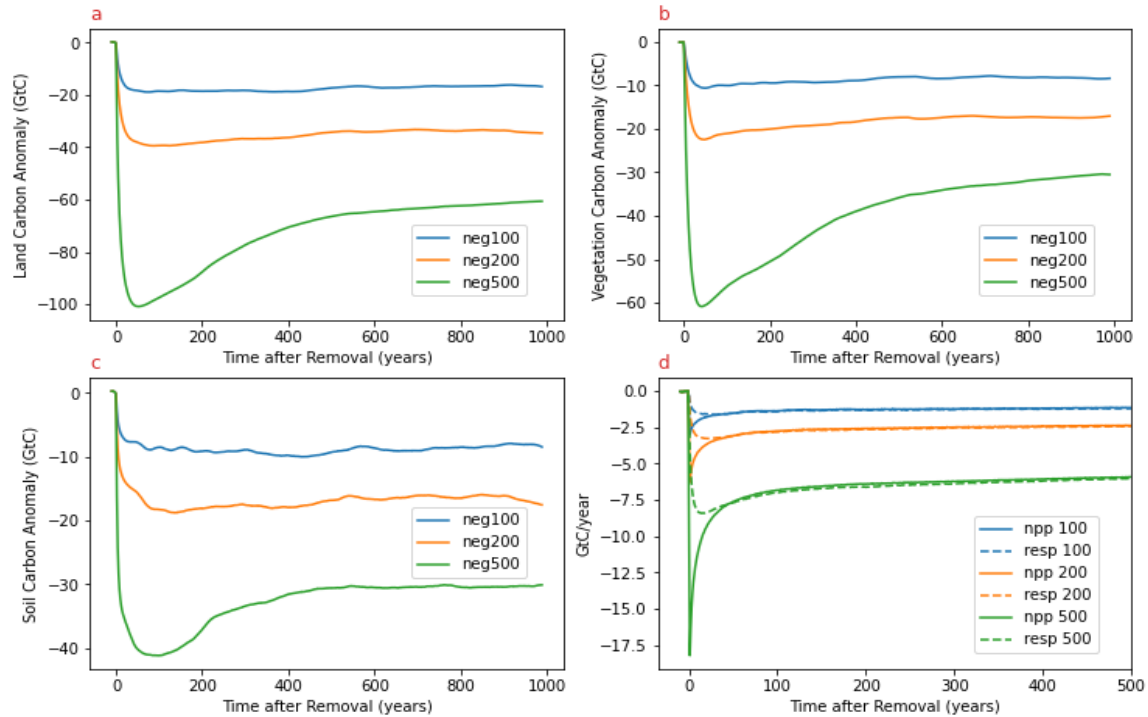
Figure 4: Land carbon anomaly (a), vegetation carbon anomaly (b), soil carbon anomaly (c), and NPP and soil respiration anomalies (d) vs time after removal for CO_2 removals of 100 GtC (blue), 200 GtC (orange), and 500 GtC (green) from the atmosphere. Anomalies are calculated with respect to one year before the removal takes place. Negative anomalies in (d) reflect the reduced rate of NPP and soil respiration after CO_2 removal. When the decline in NPP exceeds the decline in soil respiration there is a net CO_2 flux into the atmosphere. Fluxes in panel (d) are shown to the year 500 to highlight the initial response to CDR.

The land responds to changes in atmospheric CO_2 immediately following CDR. The land carbon (Figure 4a) for the neg100 and neg200 scenarios decreases immediately following CDR and remains at this lower anomaly for the remainder of the simulation. The neg500 removal scenario does gain a significant amount of land carbon after the initial loss over the course of the simulation despite a similar trajectory of atmospheric CO_2 compared to the other two scenarios. The balance of NPP and respiration (Figure 4d) controls the uptake and release of carbon on land. NPP is influenced mainly by changes in atmospheric CO_2, and respiration is controlled mainly by changes in surface air temperature, which lags changes in atmospheric CO_2. A large negative land carbon flux is seen immediately following removal (Figure A.1.) indicating that soil respiration dominates over NPP, and the land is releasing CO_2 into the atmosphere. In the neg100

and neg200 scenarios the balance between NPP and soil respiration reverses about 80 years after the removal, indicating that the land turns into a weak sink of CO_2. In the neg500 scenario the source to sink transition occurs 50 years after the removal, and the land remains a carbon sink thereafter.

When examining the vegetation (Figure 4b) and soil (Figure 4c) carbon anomalies they contribute about equally to the overall land carbon anomaly in the neg100 and neg200 simulations, but vegetation carbon contributes more to the overall land carbon anomaly in the neg500 simulation than soil carbon. In the neg500 simulation, there is a sharp decline in vegetation carbon after the removal, and a recovery that starts 50 years after the removal. Since vegetation carbon is mainly influenced by NPP, which is controlled by atmospheric CO_2, the recovery in vegetation carbon could be a response to the rebound in atmospheric CO_2 concentrations following the removal. Soil carbon exhibits an immediate, but more gradual decrease than vegetation carbon following removal. In the neg100 and neg200 scenarios, soil carbon stays at this lower level for the remainder of the simulation, while in the neg500 scenario, there is a period of about 100 years where soil carbon remains at a lower level before increasing and reaching an approximately steady state. The mechanisms driving land carbon recovery in neg500 simulation remains unclear. The soil gains carbon through leaf litter fall and loses carbon through respiration, which is controlled mainly by temperature. Soil carbon decreases shortly after removal due to a decrease in NPP, and hence a decrease in leaf litter fall. As atmospheric CO_2 recovers, NPP and leaf litter fall begin to increase while soil respiration decreases due to cooling, which may result in an increase in soil carbon in the neg500 simulation.
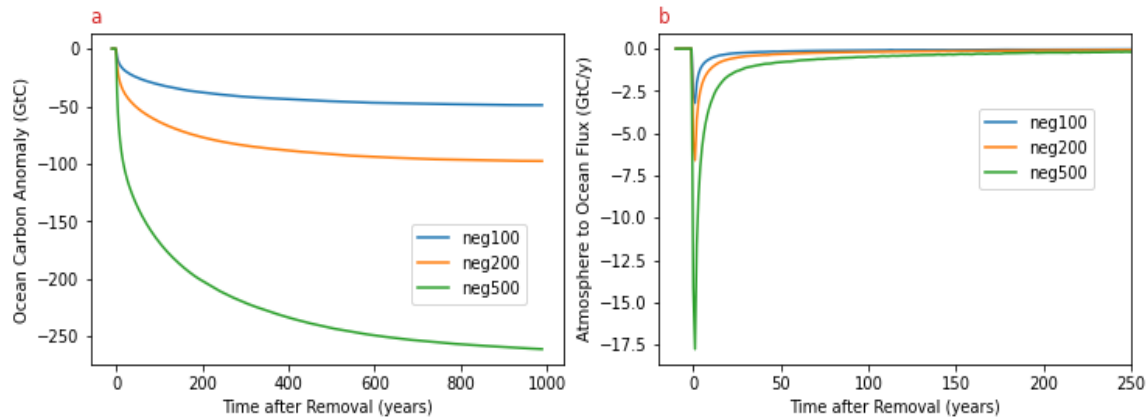
Figure 5: Ocean carbon anomaly (a), and atmosphere to ocean carbon flux (b) vs time after removal for CO_2 removals of 100 GtC (blue), 200 GtC (orange), and 500 GtC (green) from the atmosphere. Time after removal for (b) is shown to year 250 to focus on the response shortly after removal commences. A negative flux denotes carbon being released into the atmosphere from the ocean. Anomalies are calculated with respect to one year before the removal takes place.

Ocean carbon (Figure 5a) decreases for the entire simulation following the negative emission. This continuous loss of carbon is reflected in the flux of carbon into the ocean (Figure 5b). The atmosphere to ocean carbon flux remains negative for the entire simulation for all amounts of removal, indicating that the ocean carbon response to negative emissions does not equilibrate for centennial timescales. Before removal the system is in equilibrium and the flux between the atmosphere and the ocean is zero. Immediately following removal, the partial pressure gradient of CO_2 at the sea surface reverses, leading to a release of CO_2 into the atmosphere. The continuous outgassing of CO_2 by the ocean is a result of the partial pressure gradient reversal, with carbon from the deeper ocean to attempt to restore a balance with the new atmospheric CO_2 concentrations.

4.1.2. Climate-Carbon Cycle Response to 500 GtC Removal Scenarios

In the previous section, the instantaneous neg500 removal scenario shows a temperature response which exhibits a unique step-like cooling behavior after removal, and a different trajectory of carbon changes on land following CDR as compared to the other removal scenarios. This section investigates the global and spatial responses of

surface air temperature and carbon changes on land to identify the driving mechanisms behind the unique carbon and temperature trajectories in the neg500 removal scenario. Scenarios with different rates of removal are considered to explore the rate-dependence of these unique features.

4.1.2.1. Surface Temperature Response in 500 GtC Removal Scenarios
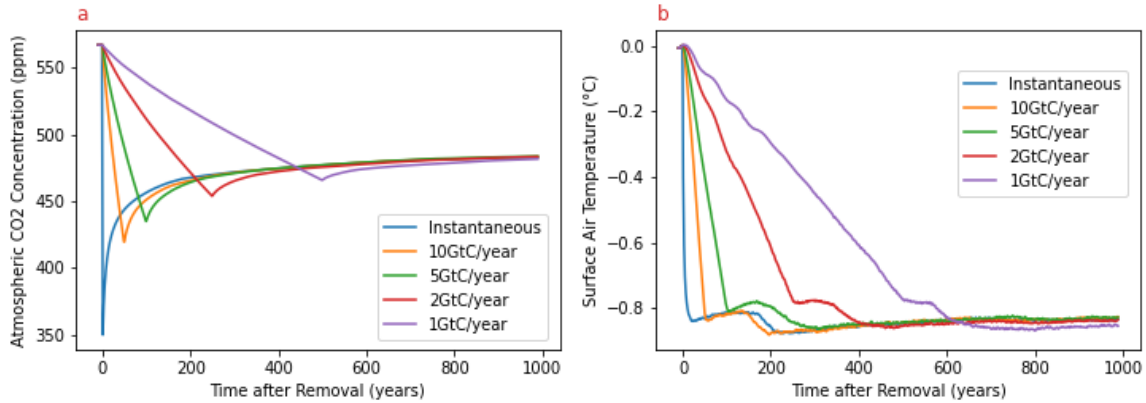
Figure 6:   Atmospheric CO_2 concentration (a) and surface air temperature (b) vs time after removal for different removal rates in the neg500 simulation. Removal rates of instantaneous (blue), 10 GtC/year (orange), 5 GtC/year (green), 2 GtC/year (red) and 1 GtC/year (purple) are shown. Anomalies are calculated with respect to one year before the removal takes place.

Each removal rate within the 500 GtC removal amount exhibits a step response in its cooling trajectory (Figure 6b) despite no additional reduction in atmospheric CO_2 (Figure 6a) following the completion of removal. A plateau or slight increase in surface air temperature occurs immediately following the completion of removal before there is a second cooling event. The first temperature plateau occurs for longer the higher the rate of removal, with the instantaneous removal scenario experiencing a plateau for almost 200 years before cooling again, and the scenarios with the slowest removal rate of 1 GtC/year experiencing a plateau for less than 100 years after removal before the secondary cooling event.
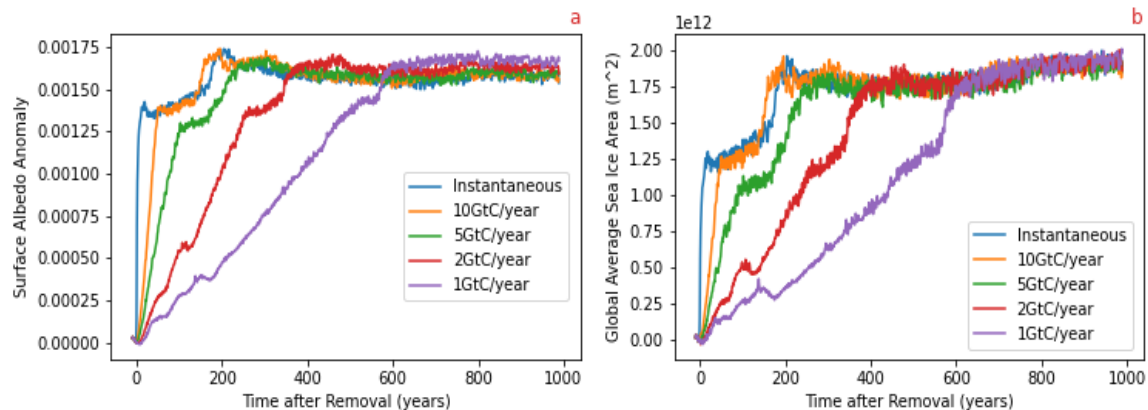
Figure 7:   Global Surface albedo anomaly (a) and global average sea ice area (b) vs time after removal for all rates in the neg500 scenario. Anomalies are calculated with respect to one year before the removal takes place.

Surface albedo changes (Figure 7a) give insight to changes in ice cover and vegetation on land and ice cover in the ocean, which could be mechanisms behind the cooling step response of surface air temperatures. The change in global surface albedo reflects the step response of the temperature trajectories, with an abrupt increase shortly after the secondary cooling event. Further investigation suggests that the abrupt albedo increase occurs over the ocean (Figure A.2.), suggesting mechanisms in the ocean as a potential driver of the abrupt cooling response in the 500 GtC scenarios.

Global sea ice area (Figure 7b) exhibits a step increase in sea ice at the same time as the step response in surface air temperatures. This indicates that increases in sea ice area are driving the changes in albedo and therefore surface air temperature for all rates of removal in the neg500 removal scenarios. Further investigation shows that the step increase in sea ice area is occurring in the Southern Hemisphere (Figure A.3.), suggesting that changes in Southern Hemisphere sea ice are driving the abrupt cooling response.
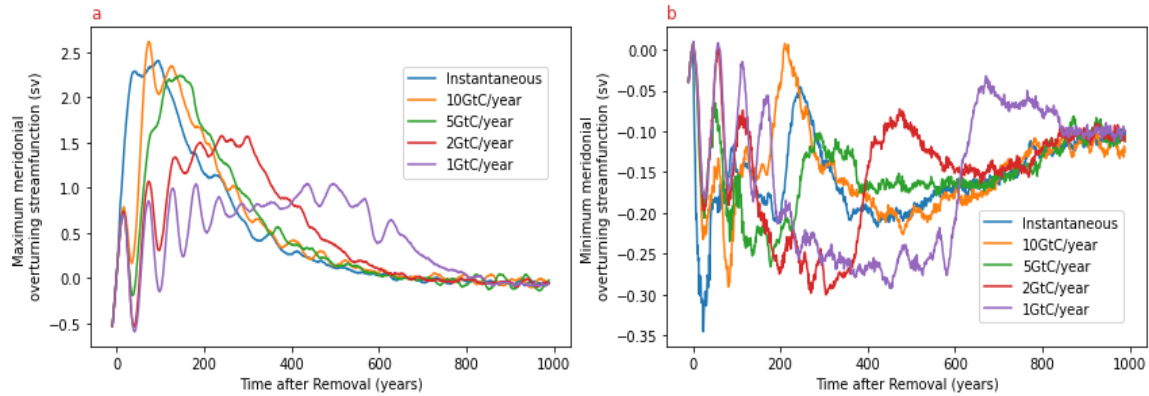
Figure 8: Maximum (a) and minimum (b) meridionial overtuning streamfunction anomalies for all rates in the neg500 removal. Units of 1 Sverdrup (Sv) = 1million m^3/s. Anomalies are calculated with respect to one year before the removal takes place.

To determine the mechanism behind the increase in sea ice area the meridional overturning stream functions are explored (Figure 8). These stream functions describe the North to South (meridional) volume of water moving through the ocean in a given time. Higher values indicate stronger ocean circulation. The maximum function indicates the strength of circulation in the North Atlantic, and is an indicator of the rate of North Atlantic Deep Water (NADW) formation. The minimum function indicates this strength in the Southern Ocean, and is an indicator of the rate of Antarctic Bottom Water (AABW) formation.

The circulation in the Southern Ocean (Figure 8b) exhibits large abrupt changes at about the same time as the southern hemisphere albedo and sea ice response, and global surface air temperature response. Minimum overturning stream-function values are low when sea ice is low, and jump to higher values when sea ice area increases. All values converge to an anomaly slightly lower than before the removal, indicating that the circulation in the Southern Ocean has decreased by the end of the simulation. Ocean circulation is linked to heat transport, both across latitudes and between the surface and deep ocean, and we hypothesize that changes in Southern Ocean circulation are associated with changes in ocean heat flux that drive the changes in sea ice.

To localize the temperature response in the neg500 removal scenario and further identify the mechanisms which are causing changes in surface air temperature, sea ice,

and ocean circulation, the spatial distribution of sea surface temperature, ventilation depth, and sea ice area are explored for the scenario with a 5 GtC/year removal (Figure 9). The difference before and after the abrupt surface air temperature change (year 150 and 300, respectively) is used to determine the spatial changes in these variables and their association with the unique cooling response in the 500 GtC removal scenarios.
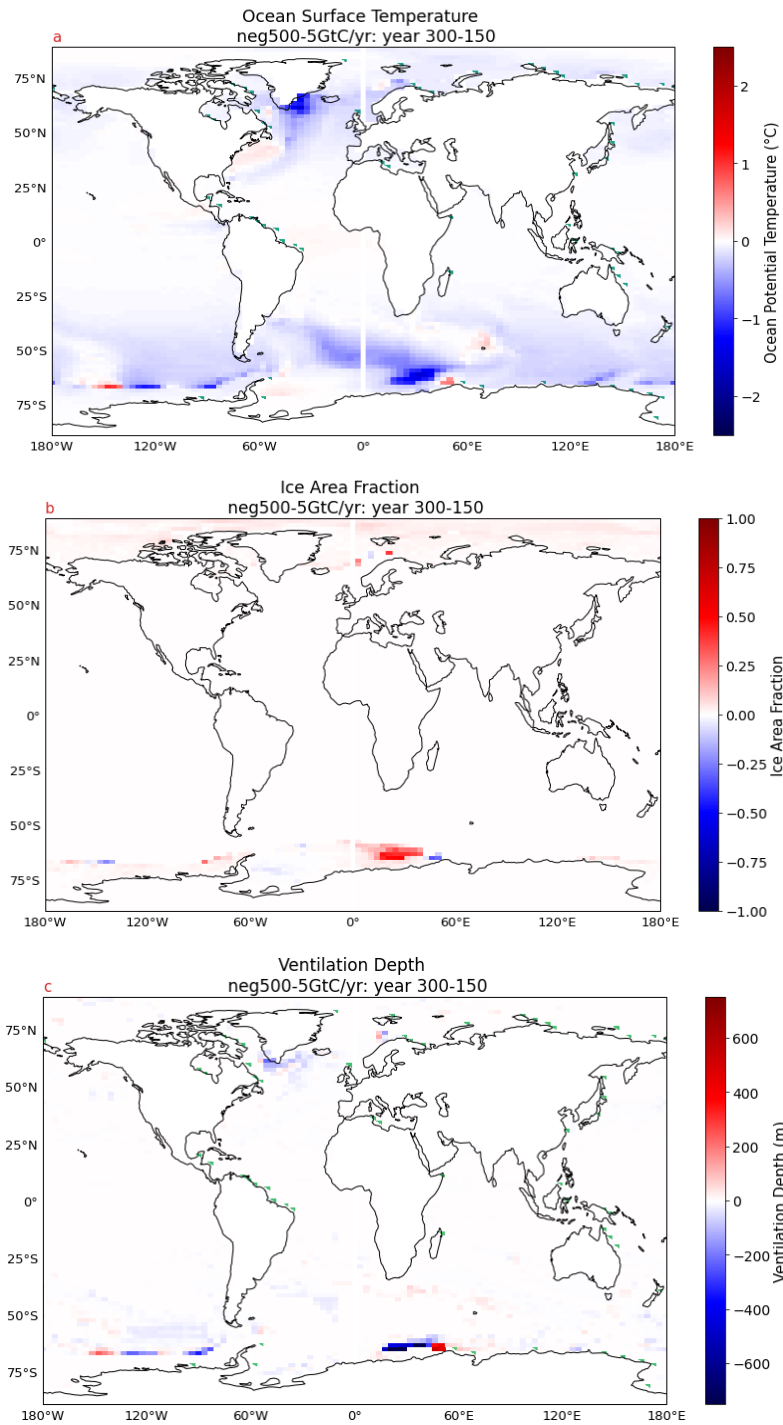
Figure 9:   Ocean surface temperature (a), ice area fraction (b), and ventilation depth (c) change from year 150 to year 300 for the neg500 5 GtC/year rate simulation. Ocean surface temperature (a) represents the first 50m of the ocean surface. Increases in are shown in red and decreases are shown in blue. Ventilation depth (c) describes the depth which ocean surface waters are carried to. Blue in this plot (c) describes areas which have deepened, and red described shallower ventilation depth.

In the Southern hemisphere there are several areas with significant cooling, particularly in the Southern Ocean between 0° and 60°E. These areas of cooling are associated with an increase in sea ice area. Ventilation depth deepens in areas which are shown to exhibit cooling, indicating deep ocean mixing is occurring in these areas. It is beyond the scope of this thesis to investigate the exact mechanisms which drive these Southern Ocean changes. It can be concluded that an abrupt cooling in the Southern Ocean creates increases in sea ice formation and surface albedo which triggers a secondary surface air temperature cooling response across all 500 GtC removal scenarios.

4.2.2.2. Land Carbon Response in 500GtC Removal Scenarios

This section investigates the spatial distribution of processes which influence changes in land carbon in the instantaneous neg500 removal scenario. First, the changes in vegetation and soil carbon from year 100 to year 500 of the simulation are presented. Next, the changes in vegetation and soil carbon in the neg500 removal scenario are divided by 2.5 and compared to the changes in soil and vegetation carbon in the instantaneous neg200 removal scenario. The comparison of the two scenarios will expose the differences that create the increase in the neg500 removal scenario land carbon trajectory. Changes are investigated between year 100 and 500 of the simulation to highlight the period of the neg500 removal scenario where land carbon is increasing the most.
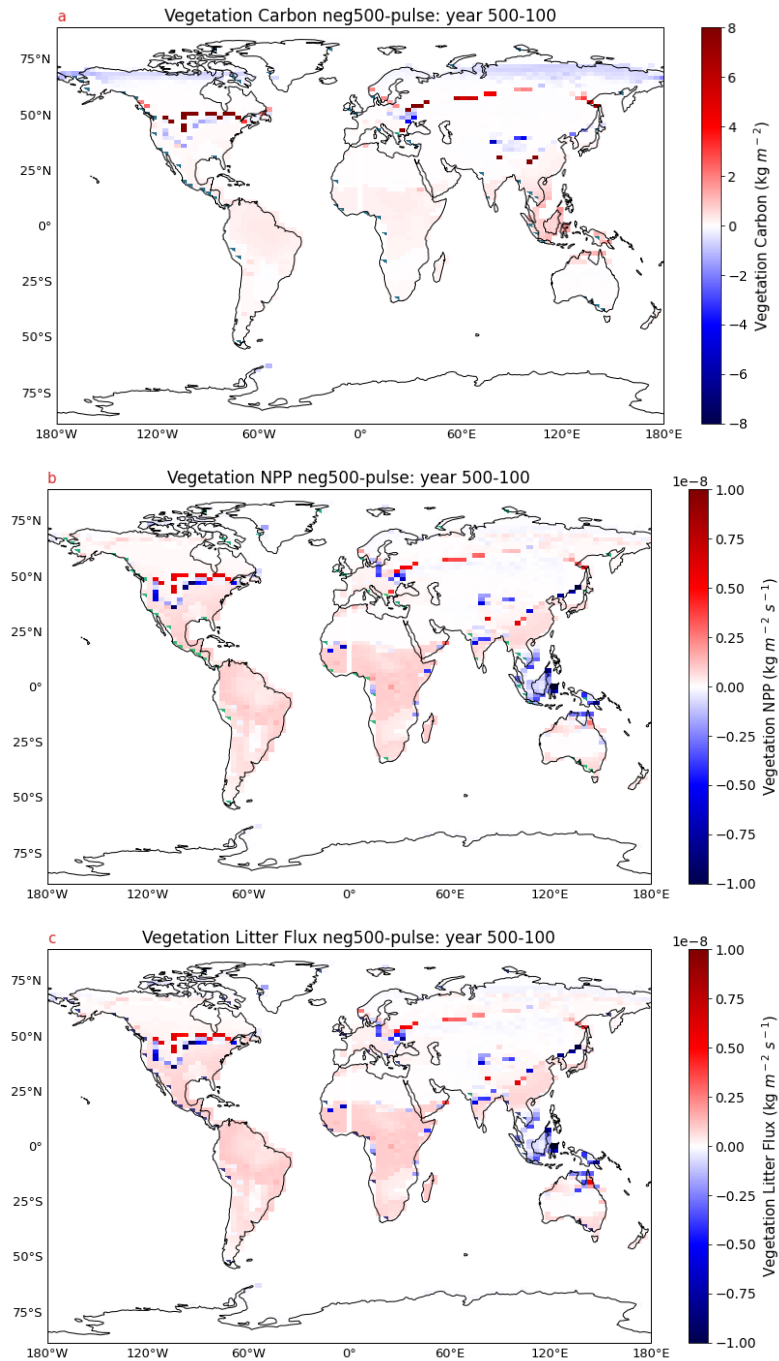
Figure 10:   Vegetation carbon (a), vegetation NPP (b), and leaf litter flux (c) changes from year 100 to 500 in the neg500 instantaneous rate of removal simulation. Gains over this period are shown in red, and losses are shown in blue.

Vegetation carbon (Figure 10a) experiences a gain in the tropics, and northern midlatitudes, and a loss in the northern high latitudes over this period. Vegetation gains

carbon through NPP (Figure 10b) and loses carbon through leaf litter flux (Figure 10c). NPP and leaf litter flux show a similar change over this period, increasing in the tropics and northern high latitudes, and decreasing in South East Asia. A decrease in NPP may indicate that there is less biomass available that could be lost through leaf litter flux, which is seen in the decrease in leaf litter flux in SE Asia, however there is an increase of vegetation carbon here despite lower NPP. Further investigation over this period reveals that the positive change shown in the vegetation carbon in SE Asia comes from an accumulation of carbon, while the positive change in the rest of the tropics comes from a decreased loss of carbon over time compared to the start of the simulation. NPP is weakening in SE Asia, which is the opposite of what is expected because increases in NPP typically indicate increases in vegetation carbon. The accumulation of vegetation carbon in South East Asia despite the decrease in NPP may come from the decrease in leaf litter flux, which allows vegetation to maintain more carbon. The increased productivity in plants in the tropics is likely due to a combination of the rebound in atmospheric carbon coupled with a decrease in temperature. Plants have an optimal temperature for growth, and the climate in the tropics at high levels of CO_2 would shift outside of that window for optimal plant growth. After removal, atmospheric CO_2 levels rebound, and temperatures decline providing a more optimal temperature for growth in the tropics while also providing higher levels of CO_2 to increase productivity in plants. Despite this mechanism, NPP in SE Asia is decreasing. To further identify mechanisms for the spatial differences between NPP and vegetation carbon, NPP is broken down by PFT (Figure 11) to show the vegetation types which contribute to this change.
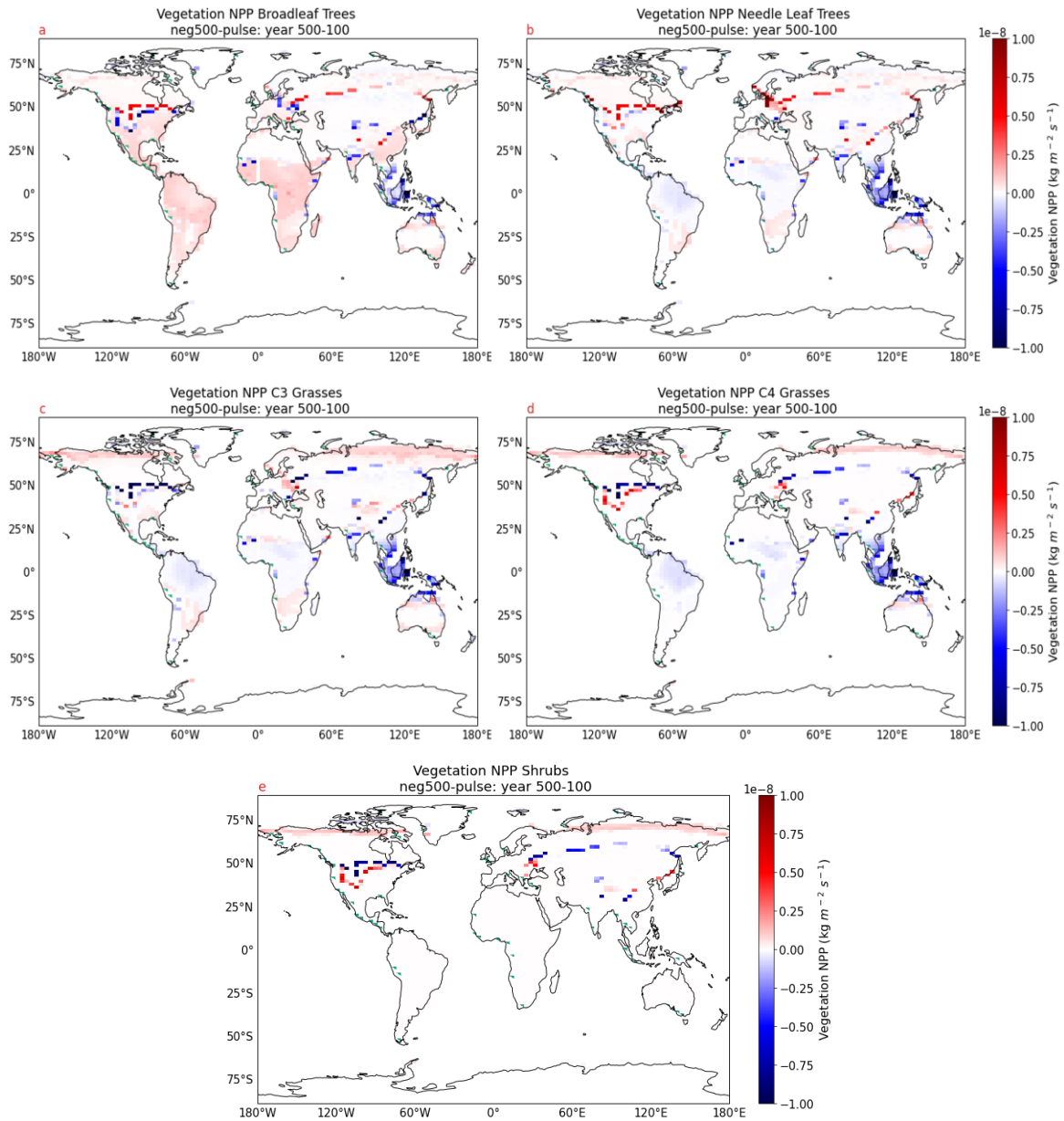
Figure 11: Vegetation NPP broken down by PFT for year 500-100 of the neg500 instantaneous rate simulation.

NPP in the tropics is decreasing for every vegetation type except for broadleaf trees. Broadleaf trees are the vegetation type which contributes the most to vegetation carbon gains in the tropics and South East Asia (Figure A.5a). There is a decrease in NPP in South East Asia in trees (Figure 11a, b) and grasses (c, d), despite the gain in vegetation carbon. Litter flux (Figure 11c) is also shown to decrease in South East Asia, indicating that less carbon is lost by the existing vegetation, further allowing carbon to

accumulate even if overall vegetation appears less productive. Grasses and shrubs are highly productive vegetation types, however they store less carbon above ground due to their decreased biomass compared to tree types. Although the productivity of grasses and shrubs appears high, the change in above ground carbon is small (Figure A.5c). This may be why there is a decrease in vegetation carbon in the northern high latitudes despite an increase in productivity in grasses and shrubs, and also may be why the large negative NPP values in South East Asia for grasses and shrubs are not reflected in the overall vegetation carbon change. Grasses and shrubs also show the largest fractional gains in vegetation in the northern high latitudes (Figure A.6), despite minimal gains in vegetation carbon, and despite no losses in the fractional coverage of trees.
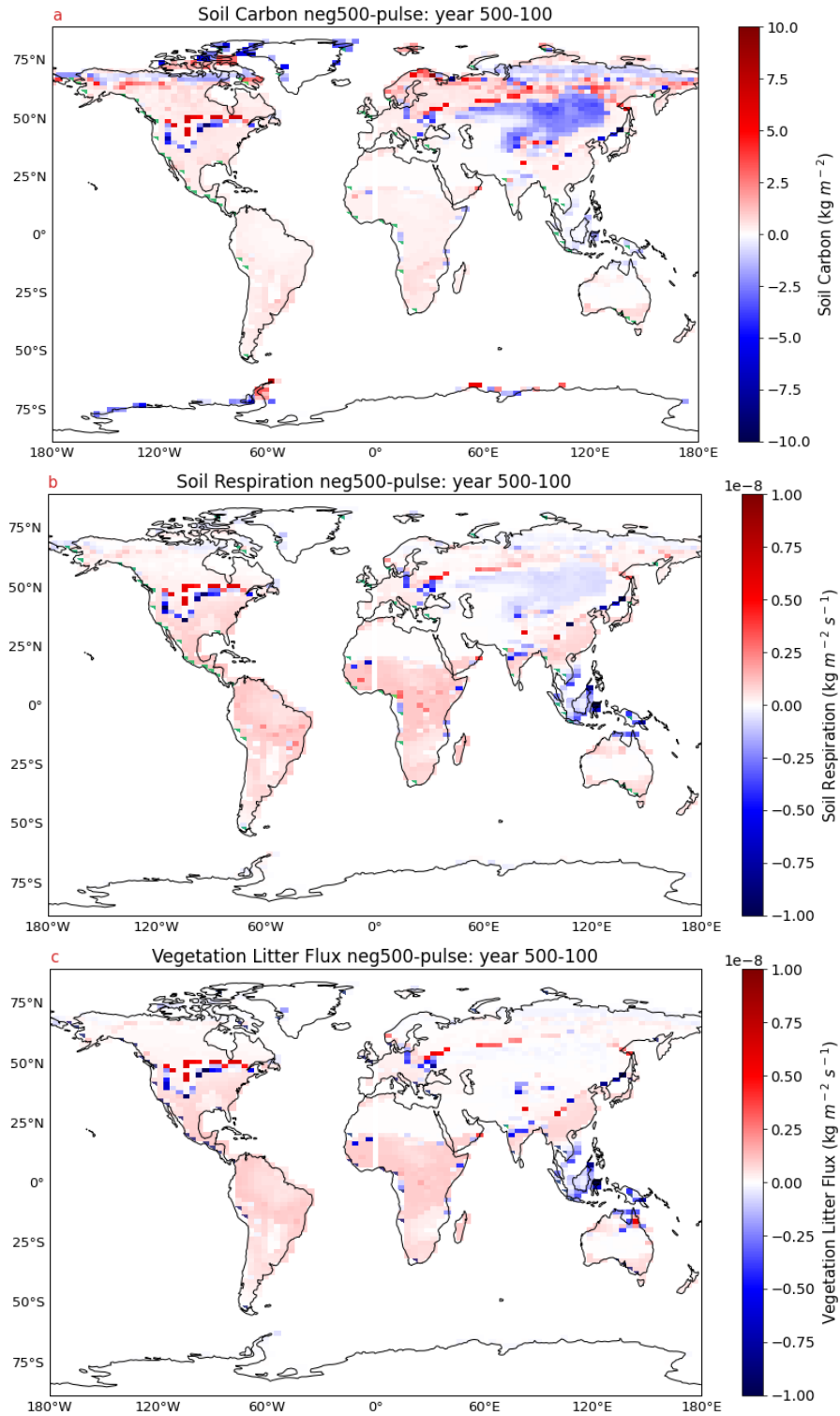
Figure 12: Soil carbon (a), soil respiration (b), and vegetation litter flux (c) changes from year 100 to 500 in the neg500 instantaneous rate simulation. Gains over this period are shown in red, and losses are shown in blue.

There is a large decrease in soil carbon (Figure 12a) and soil respiration (b) in Central Asia, but an increase in most other regions. The rate of soil respiration depends on temperature, in addition to inputs of carbon from vegetation litter flux (Figure 12c) in order for decomposition to occur. Soil respiration decreases in Central Asia as a decline in soil carbon is observed. There is not a clear decrease in vegetation litter flux to indicate that it is a mechanism of the decrease in soil carbon. However, there is an increase in vegetation fraction seen in Central Asia from C4 grasses and shrubs (Figure A.6). C4 grasses and shrubs may mine the soil for nutrients which may contribute to the loss in soil carbon and therefore the carbon available for respiration in Central Asia. In the southern hemisphere there is an increase in soil carbon as a result of increased litter flux, and an increase in soil respiration as a result of an increase in soil carbon available for decomposition. Decreasing surface air temperatures exhibited in the neg500 scenario will decrease the rate of soil respiration normally, however inputs from vegetation litter flux allow soil respiration to occur at higher rates despite decreases in temperature. South East Asia is an anomaly in the tropics with a strong decrease in soil carbon. Litter flux in Southeast Asia is shown to decrease, which is likely the mechanism behind decreasing soil carbon and respiration in this region. The mechanism driving the large decreases in soil carbon and soil respiration in Central Asia remain unclear. Soil carbon gains over this period come from the tropics and the midlatitude regions, contributing to a larger accumulation of soil carbon in the neg500 removal scenario compared to other removal amounts.
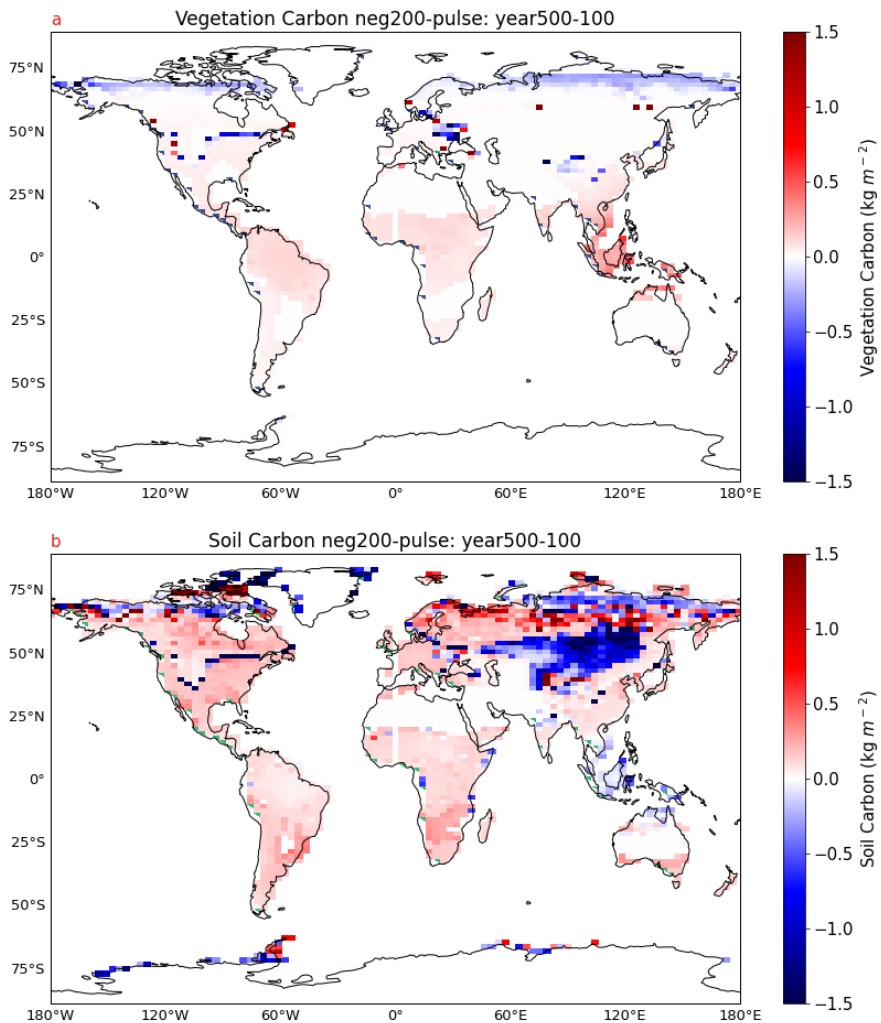
Figure 13: Vegetation (a) and soil carbon (b) changes from year 100 to year 500 for the neg200 pulse rate simulation. These plots are shown to allow a comparison of the changes which are occurring in the neg500 pulse rate simulation. Note the difference of scale between the neg200 and neg500 plots to emphasize the spatial changes in the neg200 simulation.

Vegetation and soil carbon changes in the neg200 scenario (Figure 13) show the same spatial patterns that are seen in the neg500 scenario. A loss in vegetation carbon in the northern high latitudes, and a gain in the Tropics, gains in soil carbon globally with losses in the northern high latitudes, Central and South East Asia. To compare the neg200 scenario to the neg500 scenario, vegetation and soil carbon are divided by 2.5 in the neg500 removal scenario. Then, these variables are differenced between the divided neg500 scenario and the neg200 scenario observe the difference in their land carbon responses.
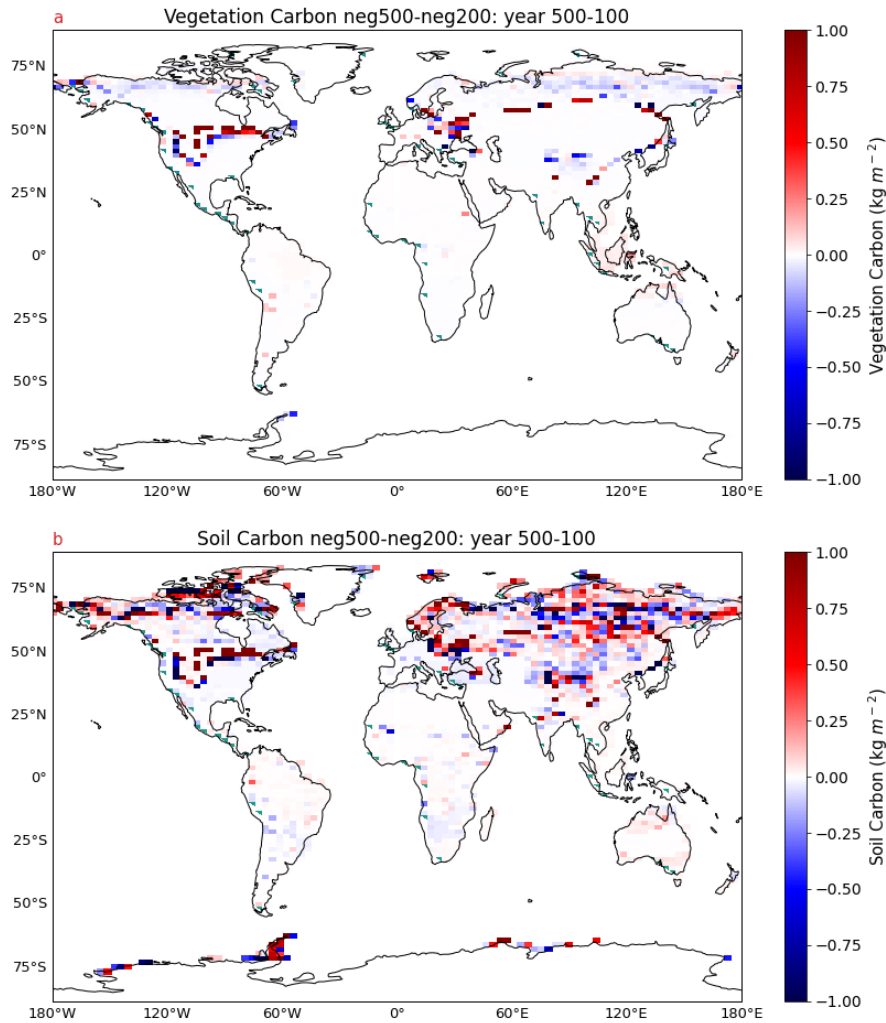
Figure 14:   Change in vegetation (a) and soil (b) carbon over year 100 to 500 difference between neg500/2.5 and neg200 pulse simulations. Red indicates areas where the neg500 simulation has higher carbon values, and blue indicates areas where vegetation and soil carbon are lower in the neg500 simulation. Note the different scale between these plots and the previous figures, scale is chosen to highlight spatial trends in the data.

The main difference in vegetation carbon between the neg500 and neg200 scenarios are the gains in the northern midlatitudes around 50 degrees N. It can be concluded that the large gains in vegetation carbon over this period in the neg500 scenario come from this midlatitude region, although there are small gains still present in the Tropics and South East Asia. In the northern midlatitudes, NPP shows trees increasing their productivity, in addition to fractional gains in vegetation (Figure A.6.) across most PFTs. The lower temperature in the neg500 simulation may have created a

more optimal environment for growth, allowing productivity to increase despite lower atmospheric CO_2 levels. Differences in soil carbon largely occur in the northern hemisphere high and mid latitude regions. The strongest gains in soil carbon occur at 50 degrees N, similar to vegetation carbon. As vegetation gains carbon it may transfer some to soils through litter flux, or distribute carbon to its roots to be stored as below ground biomass. There is no clear spatial pattern in the distribution of soil carbon that may highlight a mechanism for the difference between scenarios. The gain in land carbon of the neg500 scenario in comparison to the neg200 scenario can be attributed to soil and vegetation carbon gains in the northern midlatidude regions. The specific mechanism controlling this change is beyond the scope of this research.

4.2. Dependence of the Climate-Carbon Cycle Response on the Rate of Removal

4.2.1. Global Climate-Carbon Cycle Response

This section presents a comparison of the Earth system response for scenarios with a total removal of 200 GtC and different rates of removal. A spatial analysis is provided for the land carbon response to identify potential differences in the Earth system response between scenarios with different removal rates (section 4.2.2).
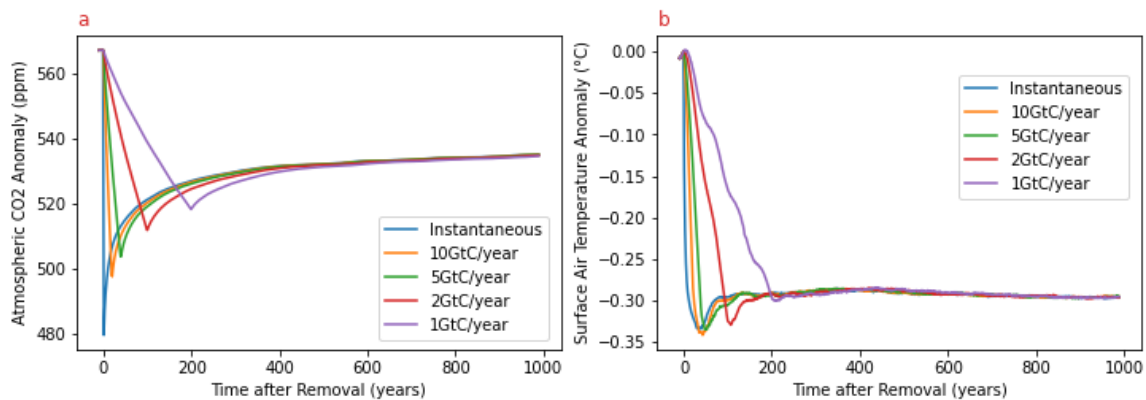
Figure 15: Atmospheric CO_2 concentration (a) and surface air temperature anomaly (°C) (b) vs time after removal for scenarios with different rates of removal and cumulative removal of 200 GtC. Anomalies are calculated with respect to one year before the removal takes place.

Each scenario reaches its minimum atmospheric CO_2 anomaly within one year of the completion of removal (e.g. year 20 for the 5 GtC/yr scenario; Figure 15a). The land and ocean respond immediately once removal begins by releasing CO_2. The scenarios with slower removal rates do not reach as low of a CO_2 anomaly as scenarios with higher rates of removal due to the response from the land and ocean releasing CO_2 as the removal is taking place. The atmospheric CO_2 concentration in each simulation experiences a rebound after the completion of removal that is larger the faster the removal rate. All simulations settle to the same CO_2 concentration of -535 ppm, which still slowly increases at the end of the simulation due to the response of ocean outgassing.

Surface air temperature starts to decline immediately following the start of the removal (Figure 15b). The minimum temperature anomaly is reached 7 to 38 years after the minimum CO_2 anomaly. This minimum temperature is reached sooner after the completion of the removal for scenarios with slower rates, and takes longest for the instantaneous rate of removal, suggesting that the temperature response cannot keep up with the decrease in atmospheric CO_2 for the faster rates of removal. Temperatures reach a lower minimum value for scenarios with higher rates of removal, with an exception for the 10GtC/year removal scenario which reaches a slightly cooler temperature than the instantaneous removal scenario. After the minimum temperature is reached, there is a rebound similar to the rebound seen in atmospheric CO_2 and temperature settles in an anomaly about -0.3°C cooler than the start of the simulation. Despite the slow increase in CO_2 after all scenarios have converged to a similar value, surface air temperature continues to slowly decline for the remainder of the simulation.
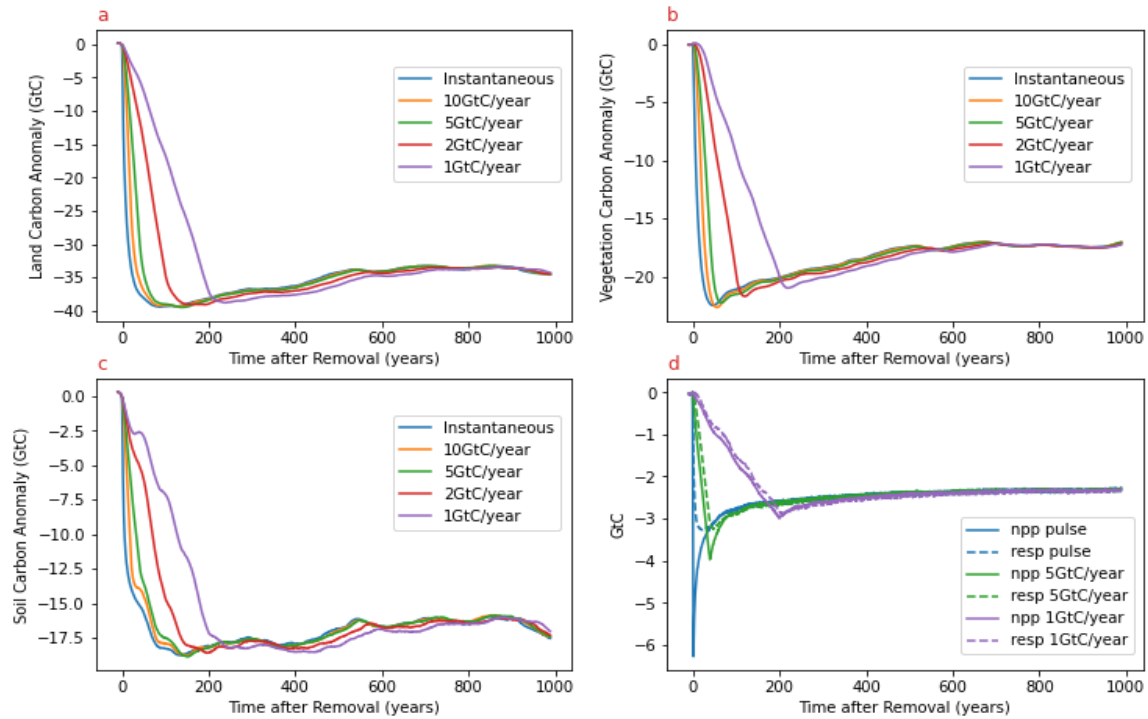
Figure 16: Land carbon anomaly (a), vegetation carbon anomaly (b), soil carbon anomaly (c), and NPP and soil respiration anomalies (d) vs time after removal scenarios with different rates of removal and cumulative removal of 200 GtC from the atmosphere. Anomalies are calculated with respect to one year before the removal takes place.

Land carbon (Figure 16a) decreases at the start of the simulation for all scenarios, indicating the land is releasing carbon into the atmosphere in response to the removal. The land is a source of carbon for approximately 90 years following removal for the instantaneous removal rate, and for 30 years following the completion of removal for the slowest removal rate. Land carbon increases slightly after it reaches its lowest point, gaining about 5 GtC from its lowest point to the end of the simulation. The slight increase in land carbon comes from both vegetation and soils (Figure 16 b, c). Vegetation and soil carbon exhibit small differences between scenarios, with scenarios with slower rates of removal generally settling at a lower value than scenarios with higher rates for several centuries after the completion of the removal. All scenarios converge to approximately the same value for vegetation and soil carbon by the end of the simulation. By the end of the simulation the land has released an average of 34.5 GtC into the atmosphere in response to the removal.
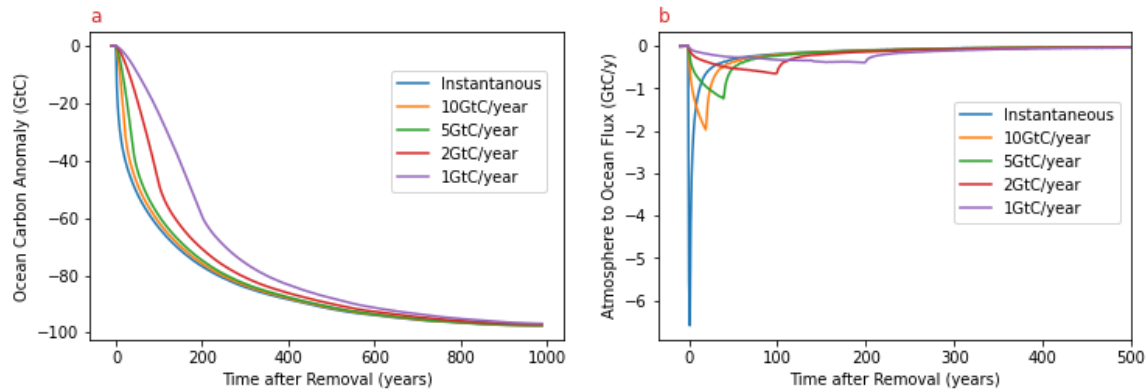
Figure 17: Ocean carbon anomaly (a) and atmosphere to ocean flux (b) vs time after removal for scenarios with different rates of removal and cumulative removal of -200 GtC from the atmosphere. Time after removal for (b) is shown to year 500 to focus on the response after removal commences. A negative flux indicates a flux into the atmosphere. Anomalies are calculated with respect to one year before the removal takes place.

Ocean carbon (Figure 17a) continues to decrease for the duration of the simulation following the completion of CO_2 removal, indicating that carbon is being released into the atmosphere. This explains the slow but continuous increase of carbon in the atmospheric CO_2 anomaly towards the end of the simulation. The decrease in ocean carbon for the entire simulation is reflected in the flux (b) which remains negative for the entire simulation, indicating the ocean is a source of carbon to the atmosphere. The atmosphere to ocean flux reaches a minimum value in the same year that atmospheric CO_2 reaches a minimum, indicating the flux of carbon out of the ocean responds immediately to decreases in atmospheric CO_2. The flux is driven by the reversal of the partial pressure gradient between the atmosphere and the surface ocean. Ocean carbon converges towards the end of the simulation (approximately year 800), which is much later than the timescale of other variables investigated in the atmosphere and on land due to the long response timescale of the ocean to changes in atmospheric CO_2. By the end of the simulation, the ocean has released an average of 97.5 GtC into the atmosphere in response to the removal.

46

4.2.2. Spatial Land Differences in 200GtC Removal Scenarios

The 200 GtC removal scenarios show very subtle differences in their vegetation and soil carbon trajectories. The following section investigates the spatial differences in vegetation carbon, soil carbon, NPP and respiration between scenarios with removal rates of 1 GtC/year and instantaneous 100 years following the completion of removal. For the instantaneous removal rate, this is year 100 of the simulation, and for the 1 GtC/year rate this is year 300 of the simulation. This analysis will explore the differences of the land carbon response to different rates of removal.
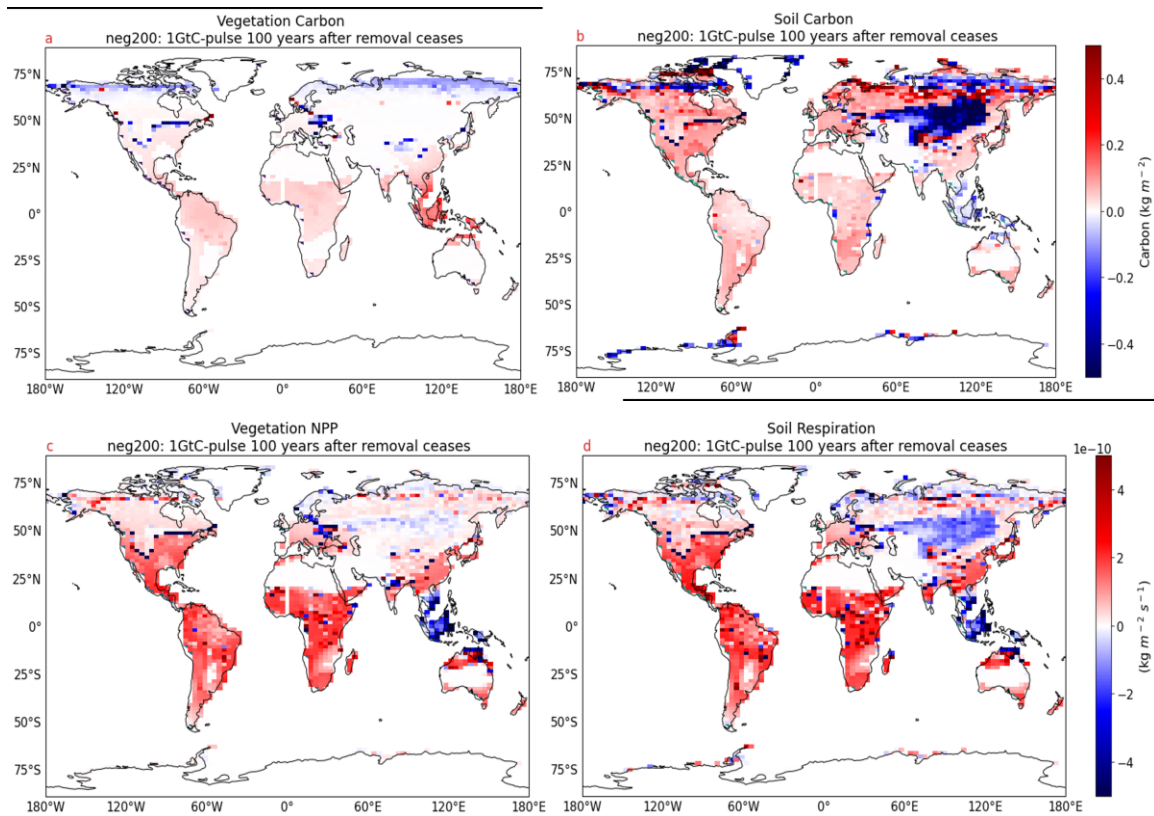
Figure 18:   Vegetation carbon (a), soil carbon (b), NPP(c) and soil respiration (d) difference between the 1 GtC and instantaneous removal rates for the 200 GtC removal scenario 100 years after the end of removal. Red areas are where the 1 GtC/year scenario shows greater values than the instantaneous removal scenario, and the blue areas are where the 1 GtC/year scenario shows lesser values than the instantaneous removal scenario.

The 1 GtC/yr removal scenario shows a larger storage of vegetation carbon in the tropics and some regions of the southern hemisphere extratropics 100 years after the end

of removal (Figure 18a). The 1 GtC/yr removal scenario shows lower values in the northern high latitudes compared to the instantaneous removal scenario. The rate of NPP is higher in the 1 GtC/yr scenario almost everywhere, except for Southeast Asia, some of eastern Europe, and Central Asia (c). The higher rates of NPP in the tropics and southern hemisphere extratropics can explain the higher vegetation carbon in these areas. An exception is the lower rate of NPP in Southeast Asia compared to an increase in vegetation carbon which is related to decreased rates of vegetation litter flux (Figure A.5.) allowing for a greater storage of vegetation carbon. There is a higher rate of NPP in the high northern latitudes coupled with a lower vegetation carbon storage in the 1 GtC/yr removal scenario. Vegetation litter flux (Figure A.6.) follows the same spatial pattern as NPP, contributing to lower vegetation carbon storage in the northern high latitudes for the 1 GtC/yr removal scenario. Lower vegetation carbon storage in the northern high latitudes for the 1 GtC/yr scenario could also be due to fewer trees and more grasses, which would result in higher NPP, litterfall, and soil carbon but less vegetation carbon.

Soil carbon (Figure 18b) is lower in the 1 GtC/yr simulation in Central and SE Asia, and the northern high latitudes. Higher NPP rates result in higher rates of vegetation leaf litter flux, which adds carbon to soils, and provides carbon for respiration to occur. If the rate of litter flux exceeds the rate of soil respiration, there will be a net gain of carbon in soils. The patterns of soil carbon and respiration follow the same areas where NPP is higher and lower, except in Central Asia and the northern high latitudes. The mechanism driving the lower soil carbon and soil respiration in Central Asia in the 1 GtC/yr scenario is unclear. Surface air temperatures are the same between the two rates at this time, so the response of soil respiration may be a result of differences in carbon input from vegetation litter flux. Soil variables in the 1 GtC/yr scenario also had 200 years longer to adjust to the onset of atmospheric CO_2 removal and surface air temperature decrease, which further presents differences in soil carbon and soil respiration between scenarios. These differences are less prominent for times after removal which are later in the simulation (Figure A.7.) and for rates of removal that are quicker than 1 GtC/year (not shown).

4.2.3. Neg100-10 GtC/year Scenario Rate Dependence

The simulation with a 10GtC/year removal rate within the 100 GtC removal scenario group shows a different temperature trajectory than the rest of the simulations within that group. The simulations with different rates in the neg200 and neg500 removal scenarios all converge to a similar atmospheric CO_2 and surface air temperature by the end of the simulation. Interestingly, even though the atmospheric CO_2 values (Figure 19a) for each rate of removal in the neg100 removal scenario converge to the same value by the end of the simulation, the temperature of the 10 GtC/yr removal scenario is slightly lower (Figure 19b) compared to the other rates of removal. The 10 GtC/yr removal scenario within this simulation group also exhibits a greater storage of carbon on land than the rest of the scenarios (Figure 20). This section investigates the spatial distribution of vegetation carbon, soil carbon, NPP and respiration to reveal the mechanisms behind the different response of the 10 GtC/yr removal scenario within the total removal of 100 GtC.
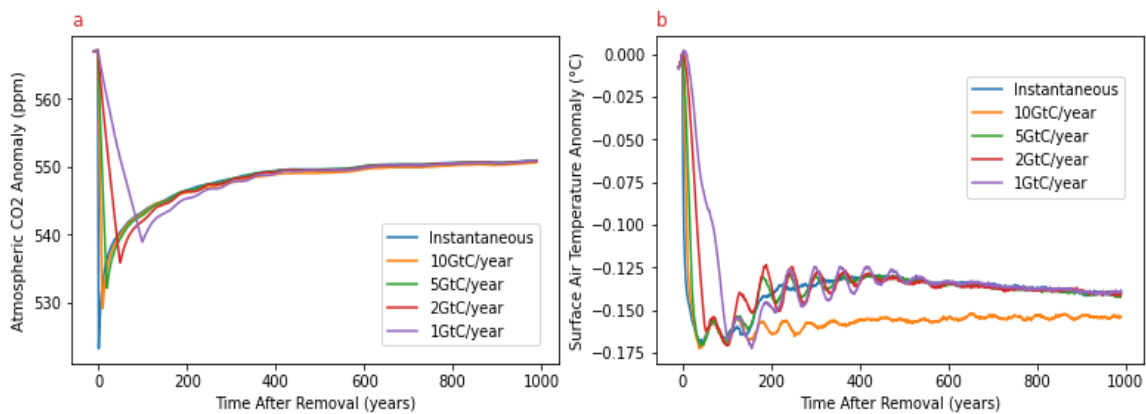
Figure 19:   Atmospheric CO_2 concentration (a) and surface air temperature anomaly (°C) (b) vs time after removal for rates of removal within the cumulative removal of 100 GtC from the atmosphere. Anomalies are calculated with respect to one year before the removal takes place.

All scenarios converge to a similar atmospheric CO_2 anomaly by the end of the simulation (Figure 19a). Despite the convergence of atmospheric CO_2, the 10 GtC/yr removal scenario shows a temperature which is -0.015°C lower than the remainder of the scenarios in this simulation at the end of the simulation. The lower temperature in the 10

GtC/yr removal scenario arises from an increase in sea ice area in the Southern Ocean as a result of ocean circulation. The mechanism which causes this temperature difference is the same as the changes in ocean circulation which influence the secondary cooling in the neg500 scenario (section 4.1.2.1). The reason why the 10 GtC/yr removal scenario is the only removal rate which triggers this response is unknown and is beyond the scope of this research.
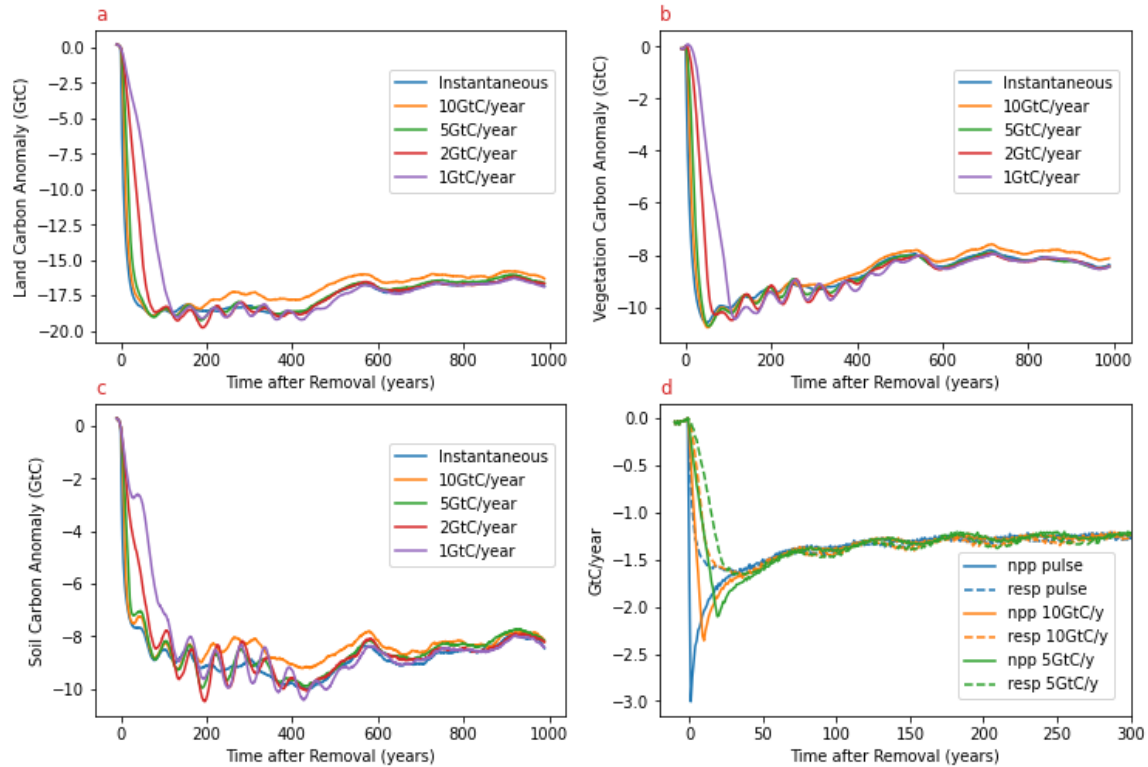
Figure 20:   Land carbon anomaly (a), vegetation carbon anomaly (b), soil carbon anomaly (c), and NPP and respiration anomalies (d) vs time after removal for all rates of removal within the cumulative removal of 100 GtC from the atmosphere. Anomalies are calculated with respect to one year before the removal takes place.

There is a small difference in the response of the 10 GtC/yr removal scenario in the storage of land carbon (Figure 20a) compared to the other scenarios in the neg100 removal simulation group. This difference begins around year 200 of the simulation, which is the same year the temperature profile of the 10 GtC/yr removal scenario diverges from the rest of the scenarios in this removal group. It is possible that Southern Ocean circulation changes cause regional temperature differences, which in turn drives

differences in the storage and transfer of carbon between vegetation, soil, and the atmosphere. The carbon storage in vegetation (b) and soils (c) shows a small difference in the 10 GtC/yr removal scenario. The difference between these simulations in soil carbon storage is slightly larger than the difference in vegetation carbon, especially in the mid range of the simulation (year 200-700). Vegetation also responds to changes in temperature, and plant productivity can increase with increasing temperatures up to an optimal temperature for plant growth. There are no large differences in the rate of NPP or respiration (Figure 20d) in the 10 GtC/yr removal scenario despite the differences in soil and vegetation carbon. Vegetation carbon is gained through photosynthesis in plants, which is the main driver behind NPP, and soil carbon is lost through respiration, so it is interesting that the 10 GtC/yr simulation shows no difference in these rates despite the difference in carbon storage in vegetation and soils.

The following section analyzes spatial differences in vegetation carbon, soil carbon, NPP and respiration between the 10 GtC/yr removal scenario and the instantaneous rate of removal within the neg100 simulation. Spatial differences are compared at 500 years after the removal is completed to determine the driving mechanisms behind the difference in the land carbon trajectory of the 10 GtC/yr removal scenario compared to the instantaneous removal scenario within the 100 GtC removal amount.
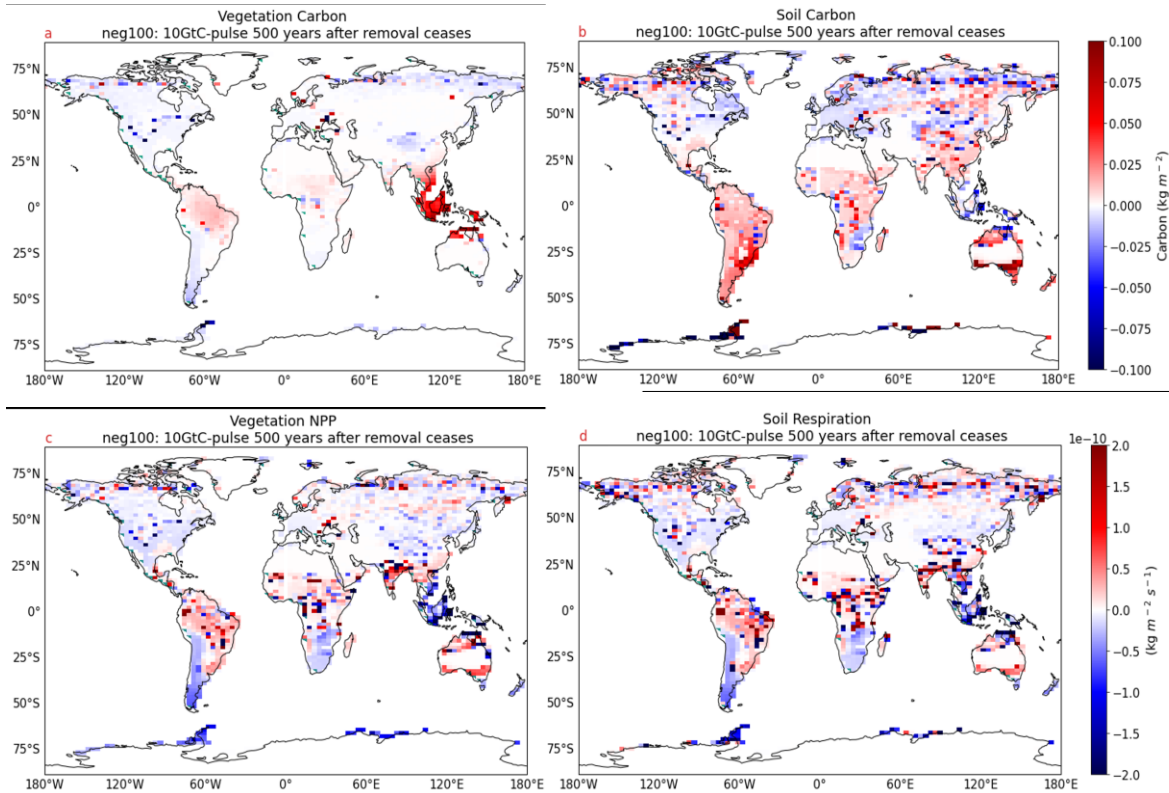
Figure 21: Vegetation carbon (a) NPP (b) soil carbon (c) and soil respiration (d) difference between the 10GtC and pulse removal rates for the 100GtC removal amount. Red areas are where the 10GtC rate shows greater values than the pulse, and the blue areas are where the 10GtC rate shows lesser values than the pulse.

Vegetation carbon (Figure 21a) exhibits higher values in the 10 GtC/yr removal scenario in the tropics, mainly South East Asia. The tropics are generally an area which experience higher rates of NPP (c) in the 10 GtC/yr removal scenario also, potentially indicating that lower temperatures may be providing plants with a more optimal temperature for growth. The opposite sign between vegetation carbon and NPP in South East Asia is related to the reduction in the rate of leaf litter flux (Figure A.9.), however the mechanism which causes this is unknown. There are lower values of vegetation carbon and NPP in the mid-high latitudes in the northern and southern hemisphere, with a slightly higher NPP in Central Asia. The higher NPP in Central Asia contributes to higher soil carbon storage (b) due to increased leaf litter flux. Lower productivity and vegetation carbon in the mid-high latitudes may come from decreased vegetation as a result of lowering temperatures possibly causing frozen ground or less optimal temperatures for

vegetation to grow. Warmer temperatures cause the earlier onset of growing seasons and cause vegetation to migrate to higher latitudes due to more optimal temperatures in areas that are typically too cold for vegetation to grow. Due to energy limitations in high latitude regions, plants are sensitive to changes in temperature (Bastos et al., 2018). Since there are lower temperatures in the 10 GtC/yr removal scenario this affects high latitude vegetation growth through limitations on the rate of the chemical reactions that cause photosynthesis and therefore NPP in plants, which reduces vegetation carbon in these regions.

Soil carbon (Figure 21b) shows higher amounts of storage in the Southern Hemisphere, tropics, and Central Asia, and lower levels of storage in the Northern midlatitudes for the 10 GtC/yr removal compared to the instantaneous removal scenario. Soil respiration (d) shows lower rates in the northern and southern midlatitudes and higher rates in the tropics. Soil carbon may be experiencing higher levels of storage in the South Africa and South America through reduced rates of respiration due to the cooler temperature profile of the 10 GtC/yr removal scenario. Higher rates of NPP in the tropics are leading to increased litter flux (Figure A.9.) which contributes to the input of carbon into soils, and allows respiration to occur at a higher rate in the 10 GtC/yr removal scenario. Soil carbon is acumulating in the tropics despite the increased rate of respiration, indicating that the input of leaf litter is greater than the loss of carbon through respiration, which is further reflected in the higher rate of NPP in this area. Lower rates of soil respiration in the Northern midlatitude regions for the 10 GtC/yr removal rate might be in part due to decreased temperatures, which allows soil carbon storage to remain high. There is an increased area of soil carbon storage in Central Asia, which also might be in part due to increased NPP and litter flux in this area. Southeast Asia shows a lower level of soil carbon and soil respiration in the 10 GtC/year removal rate due to less input of carbon from NPP and litter flux, reducing the amount of carbon available for respiration.

4.3.   Effectiveness of CDR

The effectiveness of a given CO_2 removal at drawing down atmospheric CO_2 (CRF) and cooling surface air temperatures (CE_T), defined in section 3.2.4, are used in this study. The following section compares the CRF and CE_T for a given cumulative CO_2 removal and its associated rates, and highlights differences between the effectiveness for a given amount and rate of CO_2 removal.

There is a dependence of the CRF on both the amount and rate of removal 100 years following the completion of removal (Table 3) which depends on the land and ocean response to CDR. For a given rate of removal, the CRF decreases as the amount removed increases. The 100 GtC removal scenarios have the highest CRF. There is a decrease in the CRF as the rate of removal decreases for a given removal amount. CDR in scenarios with faster rates of removal are more effective at drawing CO_2 from the atmosphere than in scenarios with slower removal rates. Although all scenarios for a given amount of removal converge to the same atmospheric CO_2 anomaly by the end of the simulation, the fraction of the rebound which has occurred 100 years after the removal has completed is less for scenarios with faster removal rates, causing the removal to have a higher CRF. As atmospheric CO_2 is being removed in scenarios with slower removal rates, the land and ocean are releasing CO_2 to counter the removal as it is taking place, decreasing the CRF 100 years following the completion of removal. This release of CO_2 from the land and ocean also decreases the level the minimum atmospheric CO_2 reaches, and the level of the rebound that occurs before converging to a common atmospheric CO_2 anomaly with other rates of removal in the same scenario grouping. CDR is most effective at drawing down atmospheric CO_2 in scenarios with the fastest rates of removal and 100 GtC cumulative removal amounts, and the least effective in scenarios with the slowest removal rates and 500 GtC cumulative removal amounts.

The differences in the CRF between scenarios with different magnitudes and rates of removal decrease the later in the simulation the CRF is calculated. If the CRF is calculated 500 years after the end of the removal, for instance, the rate dependence is negligible (Table A.1.). The rate dependence of the CRF is negligible the later it is

measured in the simulation because the Earth system has had time to respond to the cumulative changes in atmospheric CO_2 regardless of the rate of removal.

Table 3: Cumulative removal fraction (CRF) for different amounts and rates of removal. The CRF is calculated 100 years following the completion of removal for each individual amount and rate. At 100 years following the completion of removal the CRF depends on the amount and the rate of removal.

	100GtC	200GtC	500GtC
Instantaneous	0.50	0.49	0.47
10GtC/year	0.50	0.48	0.45
5GtC/year	0.49	0.47	0.44
2GtC/year	0.48	0.45	0.41
1GtC/year	0.46	0.43	0.39

The cooling effectiveness (Table 4) is slightly dependent on the amount of removal. The 200 GtC total removal scenario shows a slightly lower cooling effectiveness compared to the scenarios with 100 GtC or 500 GtC removal amounts. The higher CE_T in the 500 GtC removal simulation is a result of variability in the ocean-sea ice system, which contributes to cooler temperatures (section 4.1.2.1). The scenarios with slower removal rates for a given removal amount show a lower CE_T. This rate dependence is related to the rate dependence of the CRF, which decreases with decreasing rates of removal. More CO_2 remains out of the atmosphere for higher rates of removal at the time the CRF and the CE_T are measured. This contributes to a larger decrease in radiative forcing, and therefore surface air temperature, causing faster rates of removal to be more effective at cooling.

When the CE_T is measured at 500 years after the completion of removal, the rate dependence is negligible, except in the case of the 100 GtC, 10 GtC/year removal scenario, for which the CE_T is larger than for the other scenarios in the 100 GtC removal scenario group. The increase in the CE_T for this scenario is due to the variability in the ocean-sea ice system, which causes additional cooling. When measured 500 years after

the end of removal, the CE_T is still slightly dependent on the amount of CO_2 removal in all scenarios, and increases for increasing amounts of CO_2 removal (Table A.2).

Table 4: Cooling effectiveness (CE_T) for different amounts and rates of removal. Units are °C/TtC. CE_T is calculated 100 years following the completion of removal for each individual amount and rate. At 100 years following the completion of removal the CE_T depends slightly on the amount and rate of removal.

	100GtC	200GtC	500GtC
Instantaneous	1.65 °C/TtC	1.48 °C/TtC	1.63 °C/TtC
10GtC/year	1.63 °C/TtC	1.47 °C/TtC	1.64 °C/TtC
5GtC/year	1.55 °C/TtC	1.46 °C/TtC	1.59 °C/TtC
2GtC/year	1.49 °C/TtC	1.46 °C/TtC	1.59 °C/TtC
1GtC/year	1.48 °C/TtC	1.46 °C/TtC	1.66 °C/TtC

Chapter 5.   Discussion and Conclusions

This section provides a summary of the results presented in the previous chapter to highlight the key findings from this study. A discussion of these results in the context of the available literature is then presented, and limitations of this study identified. The last section of this chapter reflects on the significance, and implications of this study, and provides directions for future research.

5.1.   Summary of Results

5.1.1. Dependence of the Global Climate-Carbon Cycle Response on the Amount and Rate of Removal

The amplitude of the climate carbon cycle response to CO_2 removal from the atmosphere depends on the amount removed whether considering the terrestrial, oceanic, or temperature responses. As the amount of CO_2 removed increases, both the magnitude of decline of atmospheric CO_2 concentrations following removal, and the magnitude of atmospheric CO_2 concentration rebound from the minimum increases. The larger rebound in atmospheric CO_2 concentration from the minimum as the amount of CO_2 removed increases is in response to a larger release of carbon from the ocean and land at higher CO_2 removal amounts. On land, the rate of NPP is reduced more under scenarios with higher removal amounts than lower removal amounts. The reduction in NPP in response to declining atmospheric CO_2, together with the lag in the reduction of soil respiration in response to declining surface air temperature, causes a flux of carbon out of the land, which increases with increasing removal amount. In the ocean, the amount of carbon released also increases with increasing amounts of removal. The ocean continues to release carbon on centennial timescales in response to the removal for all amounts of removal. Finally, the level of atmospheric temperature decline also increases as CO_2 removal amount increases. These results highlight the dependence of the Earth system response to CO_2 removal on the amount removed.

For any given amount of CO_2 removal, the magnitude of decline in atmospheric CO_2 concentration is dependent on the rate of removal on a 100-year timescale. For

simulations with slower rates of removal, the land and ocean release CO_2 while the removal is taking place, which prevents atmospheric CO_2 from reaching the larger minimum anomalies that are achieved in scenarios with higher removal rates. After the completion of removal, the rebound in atmospheric CO_2 from the minimum is larger for faster rates of removal. All scenarios within a given amount of total CO_2 removal converge to approximately the same atmospheric CO_2 anomaly by the end of the simulation. Surface air temperature declines immediately following CO_2 removal, and reaches its minimum anomaly approximately 40 years after the minimum atmospheric CO_2 anomaly for scenarios with instantaneous removal rates. The minimum temperature anomaly occurs sooner after the minimum atmospheric CO_2 anomaly for slower removal rates. After the minimum temperature, there is a rebound similar to the rebound in atmospheric CO_2. For any given amount of total CO_2 removal, temperature anomalies converge to the same value by the end of the simulation regardless of the rate of removal.

An exception to the rate independence of CDR several centuries after the end of the removal is the 100 GtC, 10 GtC/yr simulation, which experiences a divergence in the temperature response compared to other 100 GtC simulations due to an increase in sea ice in the Southern Ocean.

5.1.2. Dependence of Spatial Patterns in Land Climate-Carbon Cycle Response on the Amount and Rate of Removal

On land, the spatial pattern of the climate-carbon cycle response 100 years following the completion of CO_2 removal depends somewhat on the rate of removal. Although differences in the global mean land carbon response between scenarios with different rates of removal are small, there are non-negligible spatial differences. These differences are of opposite sign and compensate each other, resulting in a negligible difference in the global mean response. For example, in the 200GtC removal scenarios, simulations with slower rates of CO_2 removal show a greater increase in land carbon in the tropics and Southern Hemisphere, which is compensated by a lower increase in the Northern high latitudes and Central Asia. Several hundred years after the end of the

removal, spatial differences between simulations with different CO_2 removal rates become negligible.

5.1.3. Dependence of Effectiveness on the Amount and Rate of Removal

The effectiveness of CO_2 removal at drawing down the CO_2 burden in the atmosphere is measured by the Cumulative Removal Fraction (CRF), which we define here as the reduction of the mass of carbon in the atmosphere as a fraction of the total amount of carbon removed. When evaluated 100 years after the completion of CO_2 removal, the CRF decreases as the amount of CO_2 removed increases for all rates of removal (Table 3). When the CRF is calculated at 500 years after the completion of CO_2 removal (Table A.1), the dependence of the CRF on the total amount of CO_2 removal is negligible. For a given amount of removal (i.e., 100, 200, or 500 GtC), the CRF decreases with decreasing rate of removal. However, when the CRF is calculated towards the end of the simulation (Table A.1), the dependence on the rate of CO_2 removal becomes negligible.

The effectiveness of CO_2 removal at cooling surface air temperatures is measured by the Cooling Effectiveness (CE_T), which we define here as the decrease in surface air temperature as a fraction of the total amount of carbon removed. 100 years after the completion of CO_2 removal the CE_T is slightly dependent on the amount of removal, but does not decrease monotonously with increasing amounts of removal. This dependence on the amount is due to the variability in the ocean-sea ice system, which leads to additional cooling in the 500GtC simulations. The CE_T is slightly dependent on the rate of removal, 100 years after the completion of CO_2 removal. When the CE_T is calculated later in the simulation, there is less of a dependence on the rate of CO_2 removal, however the CE_T still slightly depends on the amount of CO_2 removal (Table A.2.).

5.2. Discussion

This study presents a systematic investigation of the Earth system response to CDR as it pertains to different magnitudes and rates of removal. Previous studies find that the multi century scale Earth system response depends on the magnitude of CDR

(Jones et al., 2016; Tokarska & Zickfeld, 2015; Zickfeld et al., 2021). However, a systematic analysis of the dependence of the effectiveness of CDR in scenarios with different rates of CO_2 removal and within varying cumulative amounts has not been conducted.

Cao and Caldeira (2010) perform a large, one-time removal of all anthropogenic CO_2 from an Earth system from a transient state using version 2.8 of the UVic ESCM. Their results show a rebound in atmospheric CO_2 after CDR similar to our study. In our study, large removal amounts similar to the level of removal in Cao & Calderia (2010) result in the ocean remaining a source of CO_2 for the entire simulation, which contrasts their results in which the ocean returns into a sink of CO_2 due to the response to previous positive emissions from the transient state prior to CDR. Scenarios with any removal amount in our study show an ocean which remains a source of CO_2 for the entire simulation after instantaneous removal from the atmosphere, consistent with the ocean response for similar levels of removal from a 2xCO$_2$ equilibrium initial state in Zickfeld et al., (2021). The reduction of NPP and lagged response of respiration to CDR has been shown in previous studies (Cao & Caldeira, 2010; Jones et al., 2016; Tokarska & Zickfeld, 2015; Zickfeld et al., 2021). Our study shows the land returning to a sink of CO_2 decades after CDR for all amounts investigated, which is consistent with previous studies under similar levels of instantaneous CDR (Cao & Caldeira; Zickfeld et al., 2021). Our study shows a similar surface air temperature decline to the response shown in Zickfeld et al., (2021) for the same instantaneous CO_2 removals and initial state using a previous version of the UVic ESCM. The temperature variability exhibited in 500 GtC removal amounts in our study is not observed in the same removal scenario by Zickfeld et al, (2021).

Previous studies find that the carbon cycle response several centuries after CO_2 removal does not depend on the rate of CDR and depends only on the total amount of removal (Jones et al., 2016; Tokarska & Zickfeld, 2015; Zickfeld et al., 2021). However, the dependence of the Earth system to the amount and rate of CO_2 removal is somewhat determined by the metric used to quantify the carbon cycle response. Tokarska & Zickfeld (2015) investigate varying amounts of net negative CO_2 emissions from a

transient state using a previous version of the UVic ESCM. Their results suggest a lower effectiveness of CO_2 removal at lowering atmospheric CO_2 levels for larger removals when quantified using the AF (Table 1). However, when quantifying the same results by the PAF (Table 1) relative to a scenario without CDR, the dependence on the amount of removal is reduced. The PAF reduces to the effectiveness metric used in our study, the CRF, when using an equilibrium initial state as the reference scenario, because $\Delta CO_{2(ref)}$ is zero. We find a higher CRF for smaller cumulative CO_2 removals, similar to Tokarska & Zickfeld (2015). However, when measuring the CRF 500 years after the completion of removal, the dependence on the rate and the amount of removal is negligible (Table A.1.). Jones et al., (2016) uses the CMIP5 model ensemble to assess the effectiveness of different amounts and rates of CDR against different RCP background scenarios also finds the PAF to be insensitive of the level or timing of the negative emissions on century timescales.

Cao and Calderia (2010) calculate a cooling for removals of 100 GtC which is similar to the CE_T values shown for the 100 GtC removal amount in our study measured 100 years following the completion of removal. However, when measured 500 years after the completion of removal the cooling in their study and the CE_T in our study differs. The CE_T increases for increasing amounts of CO_2 removal at 500 years following the completion of removal (Table A.2), but does not depend on the rate of removal. This dependence arises from the Southern Ocean variability in the UVic model, which was seen in all removal scenarios under the 500 GtC removal amount, and in the 10GtC/year removal scenario under the 100 GtC removal amount.

This study highlights the differences in the regional land carbon response to different magnitudes and rates of CDR which has not previously been investigated in literature. At the regional scale, small land carbon differences of opposite sign persist 100 years following the completion of CDR between the tropics, Southeast and Central Asia, and the northern high latitudes between simulations with different rates of CO_2 removal within the same cumulative amount of removal. These results highlight how different continental regions respond to reducing atmospheric CO_2 and surface air temperature levels.

The design of the removal scenarios and the representation of the Earth system in the UVic ESCM presents some limitations in this study. The removal scenarios were applied from an Earth system in equilibrium at twice the preindustrial CO_2 concentration. Performing CDR from an equilibrium state as we have done in our study ensures an isolated response of the Earth system to CDR by removing any effects from previous positive emissions. This is an idealization, and in reality, CDR will likely take place from a transient system where we are still emitting CO_2 into the atmosphere. Although an equilibrium state allows us to isolate the Earth system response to negative emissions alone, a transient state before CO_2 removal may show a more realistic outcome of future CDR scenarios.

Variability within the UVic ESCM has affected the dependence of the Earth system response and the effectiveness of CDR on the magnitude and rate of removal. The 500 GtC removal scenarios and the 10 GtC/year removal simulation within the 100 GtC removal scenario group are both influenced by variability in the ocean-sea ice system in the Southern Ocean. This variability causes cooler temperatures in these simulations, and influences the values of the CE_T. It is possible that there would be a more monotonous dependence of the CE_T on the amount and rate of CDR in the absence of this variability.

The model was spun up without human land use change, and is referred to as a 'natural' spin up. Using a natural spin up instead of a spin up which includes land use change may overrepresent tree plant type on land, and thus overrepresent the processes involving trees compared to grass and shrub PFTs such as higher carbon storage above ground, and lower rates of NPP. Less vegetation such as trees and more shrubs and grasses if human land use change were present may lead to a difference in the CO_2 fluxes on land, which may impact the carbon cycle response to removal. However, the qualitative behavior in the global carbon cycle response to CDR in this study is expected to be robust.

The spatial pattern of the changes in land carbon on a sub-continental scale may depend on the representation of the terrestrial land surface in the UVic ESCM. Other ESMs have different representations of the land, ocean, and atmosphere which will

change the response of the Earth System to CO_2 forcing. Models have poor agreement in their representation of the land carbon cycle (Arora et al., 2020). These differences may arise from the types of vegetation represented in the model, how vegetation competes for space, the resolution of the land surface, or the nutrient cycles which are represented in the model. The UVic represents 5 PFTs, with some models representing up to 20 different PFTs (Arora et al., 2013). Nitrogen fertilization on land is represented in a simplified way in the UVic ESCM through scaling of the CO_2 fertilization by 0.7. Nitrogen is a limiting nutrient for photosynthesis in plants, which may impact the outcome of magnitude and spatial pattern of the land carbon cycle response in my analysis. In contrast to most Earth system models, the UVic ESCM represents permafrost, which may influence the land carbon response to CO_2 removal in the northern and southern high latitude regions. The qualitative global land carbon cycle response shown in this study is expected to be robust due to its representation of the fundamental processes which drive carbon fluxes on land. However, the magnitude and sub-continental spatial pattern of these results may change depending on the model used and its representation of the terrestrial carbon cycle.

In the model simulations the wind field was held fixed and did not respond to changes in temperature gradients. Neglecting changes in winds may have impacts on ocean circulation and affect ocean fluxes of heat and CO_2. This may have impacts on the magnitude of the Southern Ocean variabilities shown in my results, as changing surface air temperatures in the southern hemisphere would not influence winds. Winds influence the distribution of heat at the ocean surface and allowing changes in winds may influence the variability in the Southern Ocean and sea ice formation in the model.

The UVic ESCM does not represent clouds, which have cooling effects through the reflection of shortwave radiation emitted by the sun, and warming effects through the absorption of longwave radiation emitted by the Earth's surface. This may further impact the magnitude of the temperature response in my simulations.

5.3. Significance, Implications, and Future Research Directions

No previous research looks at the comparison between the rate and amount of CO_2 removal in a systematic way, and this is the first study of its kind using the UVic ESCM version 2.10. This research gives a clearer understanding of the dependence of Earth system response to CO_2 removal on the rate and amount of removal. Few studies have researched the isolated Earth system response to CDR by performing removals from an equilibrium initial state as we have done here. Additionally, the spatial land response to different removal rates and amounts has not been investigated previously. These results highlight highly impacted areas in terms of the changes in the land carbon response between scenarios that may be of special interest to future researchers and policy makers if they are also represented as highly impacted areas in models with different representations of the terrestrial carbon cycle under CDR. This study highlights the Northern high latitudes, tropics, and Central Asia as areas of interest.

The effectiveness metrics in this study are defined on policy relevant timescales and show that the effectiveness of CDR does depend on the rate of removal, which is a result that has not been considered in past research. Our study identifies faster rates of CO_2 removal as more effective at drawing down atmospheric CO_2 and surface air temperature per unit CDR. Policy makers will need to consider the rate of removal in future CDR implementation if we are not able to reach the climate goas specified in the Paris Agreement (Delbeke et al., 2019) . Our goals of staying below the 1.5°C threshold indicate that removals need to happen as quickly as possible to ensure the maximum effectiveness of CDR on policy relevant timescales.

The scenarios designed for this research should be tested with other models with different representations of the Earth system to determine the robustness of the Earth system response to CDR, and a further investigation into the land and ocean responses should occur to determine how the responses globally and spatially differ between models. Particularly, understanding the responses of the land carbon response to CDR in the Northern high latitudes, tropics, and Central Asia between ESMs could inform model development efforts. CO_2 removal scenarios should be initiated from different

background levels of atmospheric CO_2 to determine the Earth system response to different amounts and rates of CO_2 removal from various initial states to allow for a deeper understanding of the Earth system response to CDR. The future Earth system will most likely be in a transient state when CDR is first implemented, therefore these experiments should also be initiated from a transient state to determine the dependence of the Earth system response to different rates and amounts of CDR to show scenarios which will be more consistent with a realistic future Earth System.

References

Arora, V. K., Boer, G. J., Friedlingstein, P., Eby, M., Jones, C. D., Christian, J. R., Bonan, G., Bopp, L., Brovkin, V., Cadule, P., Hajima, T., Ilyina, T., Lindsay, K., Tjiputra, J. F., & Wu, T. (2013). Carbon-concentration and carbon-climate feedbacks in CMIP5 earth system models. *Journal of Climate*, *26*(15), 5289–5314. https://doi.org/10.1175/JCLI-D-12-00494.1

Arora, V. K., Katavouta, A., Williams, R. G., Jones, C. D., Brovkin, V., Friedlingstein, P., Schwinger, J., Bopp, L., Boucher, O., Cadule, P., Chamberlain, M. A., Christian, J. R., Delire, C., Fisher, A. R. A., Hajima, T., Ilyina, T., Joetzjer, E., Kawamiya, M., Koven, C. D., … Ziehn, T. (2020). Carbon-concentration and carbon-climate feedbacks in CMIP6 models and their comparison to CMIP5 models. *Biogeosciences*, *17*(16), 4173–4222. https://doi.org/10.5194/bg-17-4173-2020

Bastos, A., Peregon, A., Gani, É. A., Khudyaev, S., Yue, C., Li, W., Gouveia, C. M., & Ciais, P. (2018). Influence of high-latitude warming and land-use changes in the early 20th century northern Eurasian CO2 sink. *Environmental Research Letters*, *13*(6). https://doi.org/10.1088/1748-9326/aac4d3

Bitz, C. M., Holland, M. M., Weaver, A. J. and Eby, M.: Simulating the ice-thickness distribution in a coupled, J. Geophys. Res., 106(C2), 2441–2463, doi:10.1029/1999JC000113, 2001.

Boucher, O., Halloran, P. R., Burke, E. J., Doutriaux-Boucher, M., Jones, C. D., Lowe, J., Ringer, M. A., Robertson, E., & Wu, P. (2012). Reversibility in an Earth System model in response to CO2 concentration changes. *Environmental Research Letters*, *7*(2). https://doi.org/10.1088/1748-9326/7/2/024013

Boucher O, Forster PM, Gruber N, Ha-Duong M, Lawrence MG, Lenton T M, Maas A and Vaughan N E 2014 Rethinking climate engineering categorization in the context of climate change mitigation and adaptation Wiley Interdiscip. Rev. Clim. Change, 5, 23-35

Boysen, Lena R., et al. "The Limits to Global-Warming Mitigation by Terrestrial Carbon Removal." *AGU Publications*, vol. 5, May 2017, pp. 463–74, doi:10.1002/2016EF000469.

Cao, Long, and Ken Caldeira. "Atmospheric Carbon Dioxide Removal: Long-Term Consequences and Commitment." *Environ. Res. Lett*, vol. 5, no. 024011, June 2010, doi:doi:10.1088/1748-9326/5/2/024011.

Claussen, M., Mysak, L. A., Weaver, A. J., Crucifix, M., Fichefet, T., Loutre, M.-F., Weber, S. L., Alcamo, J., Alexeev, V. A., Berger, A., Calov, R., Ganopolski, A., Goosse, H., Lohmann, G., Lunkeit, F., Mokhov, I. I., Petoukhov, V., Stone, P., and Wang, Z.: Earth system models of intermediate complexity: closing the gap in the spectrum of climate system models, Clim. Dynam., 18, 579–586, 2002.

Cox, P. M. (2019). Emergent Constraints on Climate-Carbon Cycle Feedbacks. Current Climate Change Reports. https://doi.org/10.1007/s40641-019-00141-y

Cox, P. M. (2014). *Description of the TRIFFID dynamic global vegetation model Some of the authors of this publication are also working on these related projects: NERC 1.5K View project AIMES-Analysis and Integration of Modelling the Earth System View project*. *January 2001*. https://www.researchgate.net/publication/245877262

Cox, P. M., Betts, R. A., Jones, C. D., Spall, S. A., & Totterdell, I. J. (2000). Acceleration of global warming due to carbon-cycle feedbacks in a coupled climate model. *Nature*, *408*(6809), 184–187. https://doi.org/10.1038/35041539

Delbeke, J., Runge-Metzger, A., Slingenberg, Y., & Werksman, J. (2019). The paris agreement. *Towards a Climate-Neutral Europe: Curbing the Trend*, 24–45. https://doi.org/10.4324/9789276082569-2

Eby, M., Zickfeld, K., Montenegro, A., Archer, D., Meissner, K. J., & Weaver, A. J. (2009). Lifetime of anthropogenic climate change: Millennial time scales of potential CO2 and surface temperature perturbations. Journal of Climate, 22(10), 2501–2511. https://doi.org/10.1175/2008JCLI2554.1

Ehlert, D., & Zickfeld, K. (2018). Irreversible ocean thermal expansion under carbon dioxide removal. *Earth System Dynamics*, *9*(1), 197–210. https://doi.org/10.5194/esd-9-197-2018

Fanning, A.G. and A.J. Weaver. 1996. An atmospheric energy-moisture model: Climatology, interpentadal climate change and coupling to an ocean general circulation model. *J. Geophys. Res.* **101**: 15111–15128.

Friedlingstein, P., Sullivan, M. O., Jones, M. W., Andrew, R. M., & Hauck, J. (2020). *Global Carbon Budget 2020*. *2020*, 3269–3340.

Fuss, Sabine, Josep G. Canadell, et al. "Betting on Negative Emissions." *Nature Climate Change*, Sept. 2014.

Fuss, Sabine, William F. Lamb, et al. "Negative Emissions—Part 2: Costs, Potentials and Side Effects." *Environ. Res. Lett.*, vol. 13, May 2018, doi:https://doi.org/10.1088/1748-9326/aabf9f.

Fuss, Sabine. 2017 The 1.5 ∘C target, political implications, and the role of BECCS Oxf. Res. Encycl. Clim. Sci. pp 1–29

Gill, A.E. 1982. Atmosphere-Ocean Dynamics, Vol. 30 of Int. Geophys. Ser. Academic Press, New York, NY. 662 pp.

Gillett, N., Arora, V., Zickfeld, K. *et al.* Ongoing climate change following a complete cessation of carbon dioxide emissions. *Nature Geosci* **4,** 83–87 (2011). https://doi.org/10.1038/ngeo1047

Heck, Vera, et al. "Biomass-Based Negative Emissions Difficult to Reconcile with Planetary Boundaries." *Nature Climate Change*, vol. 8, 2018, pp. 151–55, doi:doi:10.1038/s41558-017-0064-y.

Held, I. M., Winton, M., Takahashi, K., Delworth, T., Zeng, F., & Vallis, G. K. (2010). Probing the fast and slow components of global warming by returning abruptly to preindustrial forcing. *Journal of Climate*, *23*(9), 2418–2427. https://doi.org/10.1175/2009JCLI3466.1

Houghton, RA. "The Contemporary Carbon Cycle." *Treatise on Geochemistry*, 2nd Edition, Elsevier Ltd, 2014, pp. 399–435, http://dx.doi.org/10.1016/B978-0-08-095975-7.00810-X.

IPCC, 2018: Summary for Policymakers. In: Global Warming of 1.5°C. An IPCC Special Report on the impacts of global warming of 1.5°C above pre-industrial levels and related global greenhouse gas emission pathways, in the context of strengthening the global response to the threat of climate change, sustainable development, and efforts to eradicate poverty [Masson-Delmotte, V., P. Zhai, H.-O. Pörtner, D. Roberts, J. Skea, P.R. Shukla, A. Pirani, W. Moufouma-Okia, C. Péan, R. Pidcock, S. Connors, J.B.R. Matthews, Y. Chen, X. Zhou, M.I. Gomis, E. Lonnoy, T. Maycock, M. Tignor, and T. Waterfield (eds.)]. In Press.

IPCC CH9 2013: Flato, G., J. Marotzke, B. Abiodun, P. Braconnot, S.C. Chou, W. Collins, P. Cox, F. Driouech, S. Emori, V. Eyring, C. Forest, P. Gleckler, E. Guilyardi, C. Jakob, V. Kattsov, C. Reason and M. Rummukainen, 2013: Evaluation of Climate Models. In: Climate Change 2013: The Physical Science Basis. Contribution of Working Group I to the Fifth Assessment Report of the Intergovernmental Panel on Climate Change [Stocker, T.F., D. Qin, G.-K. Plattner, M. Tignor, S.K. Allen, J. Boschung, A. Nauels, Y. Xia, V. Bex and P.M. Midgley (eds.)]. Cambridge University Press, Cambridge, United Kingdom and New York, NY, USA.

IPCC, 2013: Summary for Policymakers. In: Climate Change 2013: The Physical Science Basis. Contribution of Working Group I to the Fifth Assessment Report of the Intergovernmental Panel on Climate Change [Stocker, T.F., D. Qin, G.-K. Plattner, M. Tignor, S.K. Allen, J. Boschung, A. Nauels, Y. Xia, V. Bex and P.M. Midgley (eds.)]. Cambridge University Press, Cambridge, United Kingdom and New York, NY, USA.

Jones, CD., et al. "Simulating the Earth System Response to Negative Emissions." *Environ. Res. Lett.* 11, no. 095012 (2016). https://doi.org/doi:10.1088/1748-9326/11/9/095012.

Keller, David P., et al. "The Effects of Carbon Dioxide Removal on the Carbon Cycle." *Current Climate Change Reports* 4 (2018): 250–65. https://doi.org/10.1007/s40641-018-0104-3.

Keller, D. P., Oschlies, A., & Eby, M. (2012). A new marine ecosystem model for the University of Victoria earth system climate model. *Geoscientific Model Development*, *5*(5), 1195–1220. https://doi.org/10.5194/gmd-5-1195-2012

Leaky, Andrew D. B., et al. "Elevated CO2 Effects on Plant Carbon, Nitrogen, and Water Relations: Six Important Lessons from FACE." *Journal of Experimental Botany*, vol. Vol. 60, no. No. 10, 2009, pp. 2859–2876, doi:doi:10.1093/jxb/erp096.

LeQuéré, C., Andrew, R., Friedlingstein, P., Sitch, S., Hauck, J., Pongratz, J., … Zheng, B. (2018). Global Carbon Budget 2018. Earth System Science Data, Vol. 10, pp. 2141–2194. https://doi.org/10.5194/essd-10-2141-2018

MacDougall, A. H., Frölicher, T. L., Jones, C. D., Rogelj, J., DamonMatthews, H., Zickfeld, K., Arora, V. K., Barrett, N. J., Brovkin, V., Burger, F. A., Eby, M., Eliseev, A. V., Hajima, T., Holden, P. B., Jeltsch-Thömmes, A., Koven, C., Mengis, N., Menviel, L., Michou, M., … Ziehn, T. (2020). Is there warming in the pipeline? A multi-model analysis of the Zero Emissions Commitment from CO2. *Biogeosciences*, *17*(11), 2987–3016. https://doi.org/10.5194/bg-17-2987-2020

Macdougall, A. H. (2013). Reversing climate warming by artificial atmospheric carbon-dioxide removal: Can a Holocene-like climate be restored? *Geophysical Research Letters*, *40*(20), 5480–5485. https://doi.org/10.1002/2013GL057467

Mathesius, Sabine, et al. "Long-Term Response of Oceans to CO2 Removal from the Atmosphere." *Nature Climate Change*, vol. 3, Aug. 2015, pp. 1107–13

Matthews, H. D., & Caldeira, K. (2008). Stabilizing climate requires near-zero emissions. *Geophysical Research Letters*, *35*(4), 1–5. https://doi.org/10.1029/2007GL032388

Matthews, H. D., Weaver, A. J., Meissner, K. J., Gillett, N. P., and Eby, M.: Natural and anthropogenic climate change: incorporating historical land cover change, vegetation dynamics and the global carbon cycle, Clim. Dynam., 22, 461–479, doi:10.1007/s00382-004-0392-2, 2004.

Matthews, H.D., N. Gillett, P. A. Stott, and K. Zickfeld (2009): The proportionality of global warming to cumulative carbon emissions, Nature, 459, 829-833

McGuffie K. and Henderson-Sellers A. The Climate Modelling Primer, 4th Edition. Wiley-Blackwell, 2014.

Meissner, K. J., A. J. Weaver, H.D.Matthews, and P.M. Cox, 2003: The role of land surface dynamics in glacial inception: A study with the UVic Earth System model. Climate Dyn., 21, 515–537.

Meinshausen, M., Smith, S. J., Calvin, K., Daniel, J. S., Kainuma, M. L. T., Lamarque, J., Matsumoto, K., Montzka, S. A., Raper, S. C. B., Riahi, K., Thomson, A., Velders, G. J. M., & van Vuuren, D. P. P. (2011). The RCP greenhouse gas concentrations and their extensions from 1765 to 2300. *Climatic Change*, *109*(1), 213–241. https://doi.org/10.1007/s10584-011-0156-z

Meinshausen, M., Nicholls, Z. R. J., Lewis, J., Gidden, M. J., Vogel, E., Freund, M., Beyerle, U., Gessner, C., Nauels, A., Bauer, N., Canadell, J. G., Daniel, J. S., John, A., Krummel, P. B., Luderer, G., & Meinshausen, N. (2020). *The shared socio-economic pathway (SSP) greenhouse gas concentrations and their extensions to 2500*. 3571–3605.

Mengis, N., Keller, D., MacDougall, A., Eby, M., Wright, N., Meissner, K., Oschlies, A., Schmittner, A., & Zickfeld, K. (2020). Evaluation of the University of Victoria Earth System Climate Model version 2.10 (UVic ESCM 2.10). *Geoscientific Model Development Discussions*, *10*(February), 1–28. https://doi.org/10.5194/gmd-2019-373

Meyerholt, J., Sickel, K., & Zaehle, S. (2020). Ensemble projections elucidate effects of uncertainty in terrestrial nitrogen limitation on future carbon uptake. *Global Change Biology*, *26*(7), 3978–3996. https://doi.org/10.1111/gcb.15114

Millennium Ecosystem Assessment. 2005 "Scenarios". www.MAweb.org.

Minx, Jan C., et al. "Negative Emissions—Part 1: Research Landscape and Synthesis." *Environ. Res. Lett.*, vol. 13, no. 063001, May 2018, doi:https://doi.org/10.1088/1748-9326/aabf9b.

Nabuurs G J et al. 2007 Forestry climate change 2007: mitigation Contribution of Working Group III to the Fourth Assessment Report of the Intergovernmental Panel on Climate Change ed B Metz, O R Davidson, P R Bosch, R Dave and L A Meyer (Cambridge: Cambridge University Press)

Pacala, Stephen, et al. "Negative Emissions Technologies and Reliable Sequestration: A Research Agenda." *National Academies of Sciences, Engineering, and Medicine*, Oct. 2018, http://www.nationalacademies.org/basc

Pacanowski, R. 1995. MOM 2 Documentation User's Guide and Reference Manual, GFDL Ocean Group Technical Report. NOAA, GFDL. Princeton. 232 pp.

Parry, M.L., O.F. Canziani, J.P. Palutikof and Co-authors 2007: Technical Summary. Climate Change 2007: Impacts, Adaptation and Vulnerability. Contribution of Working Group II to the Fourth Assessment Report of the Intergovernmental Panel on Climate Change, M.L. Parry, O.F. Canziani, J.P. Palutikof, P.J. van der Linden and C.E. Hanson, Eds., Cambridge University Press, Cambridge, UK, 23-78.

Peixoto, J.P. and A.H. Oort. 1992. Physics of Climate. American Institute of Physics, New York. 520 pp.

Rahmstorf, S. (2002). Ocean circulation and climate during the past 120,000 years. *Nature*, *419*(6903), 207–214. https://doi.org/10.1038/nature01090

Raich, JW et al. "Respiration in Terrestrial Ecosystems." *Treatise on Geochemistry*, 2nd Edition, 2014 Elsevier Ltd, 2013, pp. 615–32, http://dx.doi.org/10.1016/B978-0-08-095975-7.00817-2.

Riahi, K., van Vuuren, D. P., Kriegler, E., Edmonds, J., O'Neill, B. C., Fujimori, S., Bauer, N., Calvin, K., Dellink, R., Fricko, O., Lutz, W., Popp, A., Cuaresma, J. C., KC, S., Leimbach, M., Jiang, L., Kram, T., Rao, S., Emmerling, J., … Tavoni, M. (2017). The Shared Socioeconomic Pathways and their energy, land use, and greenhouse gas emissions implications: An overview. *Global Environmental Change*, *42*, 153–168. https://doi.org/10.1016/j.gloenvcha.2016.05.009

Rogelj, J., Shindell, D., Jiang, K., & Fifita, S. (2018). IPCC 2018, cap2. *Global Warming of 1.5°C. An IPCC Special Report [...]*, 2.

Rogelj, J., Forster, P. M., Kriegler, E., Smith, C. J., & Séférian, R. (2019). Estimating and tracking the remaining carbon budget for stringent climate targets. *Nature*, *571*(7765), 335–342. https://doi.org/10.1038/s41586-019-1368-z

Rogelj, J., Popp, A., Calvin, K. V., Luderer, G., Emmerling, J., Gernaat, D., Fujimori, S., Strefler, J., Hasegawa, T., Marangoni, G., Krey, V., Kriegler, E., Riahi, K., Van Vuuren, D. P., Doelman, J., Drouet, L., Edmonds, J., Fricko, O., Harmsen, M., … Tavoni, M. (2018). Scenarios towards limiting global mean temperature increase below 1.5 °c. *Nature Climate Change*, *8*(4), 325–332. https://doi.org/10.1038/s41558-018-0091-3

Sanderson, B. M., & Fisher, R. A. (2020). A fiery wake-up call for climate science. *Nature Climate Change*, *10*(3), 173–174. https://doi.org/10.1038/s41558-020-0712-5

Schuur, E. A. G., McGuire, A. D., Schädel, C., Grosse, G., Harden, J. W., Hayes, D. J., Hugelius, G., Koven, C. D., Kuhry, P., Lawrence, D. M., Natali, S. M., Olefeldt, D., Romanovsky, V. E., Schaefer, K., Turetsky, M. R., Treat, C. C., & Vonk, J. E. (2015). Climate change and the permafrost carbon feedback. *Nature*, *520*(7546), 171–179. https://doi.org/10.1038/nature14338

Smith, Pete, et al. "Biophysical and Economic Limits to Negative CO2 Emissions." *Nature Climate Change*, vol. 6, Jan. 2016, DOI: 10.1038/NCLIMATE2870.

Smith P et al 2007 Agriculture Climate change 2007: mitigation of climate change. Contribution ofWorkingGroup III to the Fourth AssessmentReport ofthe Intergovernmental Panel on Climate Change ed B Metz, O R Davidson, P R Bosch, R Dave and L AMeyer (Cambridge: Cambridge University Press)

Schmittner A, Oschlies A, Matthews H D and Galbraith E D 2008 Future changes in climate, ocean circulation, ecosystems and biogeochemical cycling simulated for a business-as-usual CO2 emissions scenario until year 4000 AD Global Biogeochem. Cycles 22 GB1013

SSP Public Database Version 2.0: Keywan Riahi, Detlef P. van Vuuren, Elmar Kriegler, Jae Edmonds, Brian C. O'Neill, Shinichiro Fujimori, Nico Bauer, Katherine Calvin, Rob Dellink, Oliver Fricko, Wolfgang Lutz, Alexander Popp, Jesus Crespo Cuaresma, Samir KC, Marian Leimbach, Leiwen Jiang, Tom Kram, Shilpa Rao, Johannes Emmerling, Kristie Ebi, Tomoko Hasegawa, Petr Havlík, Florian Humpenöder, Lara Aleluia Da Silva, Steve Smith, Elke Stehfest, Valentina Bosetti, Jiyong Eom, David Gernaat, Toshihiko Masui, Joeri Rogelj, Jessica Strefler, Laurent Drouet, Volker Krey, Gunnar Luderer, Mathijs Harmsen, Kiyoshi Takahashi, Lavinia Baumstark, Jonathan C. Doelman, Mikiko Kainuma, Zbigniew Klimont, Giacomo Marangoni, Hermann Lotze-Campen, Michael Obersteiner, Andrzej Tabeau, Massimo Tavoni. "The Shared Socioeconomic Pathways and their energy, land use, and greenhouse gas emissions implications: An overview", Global Environmental Change, Volume 42, Pages 153-168, 2017, ISSN 0959-3780, DOI:110.1016/j.gloenvcha.2016.05.009

Stocker, T. F., & Wright, D. G. (1991). Rapid Transitions of the ocean's deep circulation induced by changes in surface water fluxes. *Letters to Nature*, *May*, 729–732.

Tokarska, Katarzyna B., and Kirsten Zickfeld. "The Effectiveness of Net Negative Carbon Dioxide Emissions in reversing Anthropogenic Climate Change." *Environ. Res. Lett.*, vol. 10, Sept. 2015, doi:10.1088/1748-9326/10/9/094013.

Turetsky, M. R., Abbott, B. W., Jones, M. C., Anthony, K. W., Olefeldt, D., Schuur, E. A. G., Grosse, G., Kuhry, P., Hugelius, G., Koven, C., Lawrence, D. M., Gibson, C., Sannel, A. B. K., & McGuire, A. D. (2020). Carbon release through abrupt permafrost thaw. *Nature Geoscience*, *13*(2), 138–143. https://doi.org/10.1038/s41561-019-0526-0

UNFCCC: United Nations Framework Convention on Climate Change 2015 Paris Agreement.

van Vuuren, D. P., Edmonds, J., Kainuma, M., Riahi, K., Thomson, A., Hibbard, K., Hurtt, G. C., Kram, T., Krey, V., Lamarque, J. F., Masui, T., Meinshausen, M., Nakicenovic, N., Smith, S. J., & Rose, S. K. (2011). The representative concentration pathways: An overview. *Climatic Change*, *109*(1), 5–31. https://doi.org/10.1007/s10584-011-0148-z

Vichi, M., A. Navarra, and P. G. Fogli. "Adjustment of the Natural Ocean Carbon cycle to Negative Emission Rates." *Climatic Change* 118, no. 105–118 (2013). https://doi.org/DOI 10.1007/s10584-012-0677-0

Weaver, A. J., Eby, M., Wiebe, E. C., Ewen, T. L., Fanning, A. F., MacFadyen, A., Matthews, H. D., Meissner, K. J., Saenko, O., Schmittner, A., Yoshimori, M., Bitz, C. M., Holland, M. M., Duffy, P. B., & Wang, H. (2001). The UVic earth system climate model: Model description, climatology, and applications to past, present and future climates. *Atmosphere - Ocean*, *39*(4), 361–428. https://doi.org/10.1080/07055900.2001.9649686

Zickfeld, K., Azevedo, D., Mathesius, S. *et al.* Asymmetry in the climate–carbon cycle response to positive and negative CO_2 emissions. *Nat. Clim. Chang.* **11,** 613–617 (2021). https://doi.org/10.1038/s41558-021-01061-2

Zickfeld, K., Eby, M., Matthews, H. D., Weaver, A. J., Schellnhuber, H. J., Zickfeld, K., Ebyaf, M., Matthews, H. D., & Weaver, A. J. (2009). Setting cumulative emissions targets to reduce the risk of dangerous climate change. *106*(38), 16129–16134.

Zickfeld, K., MacDougall, A. H., & Damon Matthews, H. (2016). On the proportionality between global temperature change and cumulative CO2 emissions during periods of net negative CO2 emissions. *Environmental Research Letters*, *11*(5). https://doi.org/10.1088/1748-9326/11/5/055006

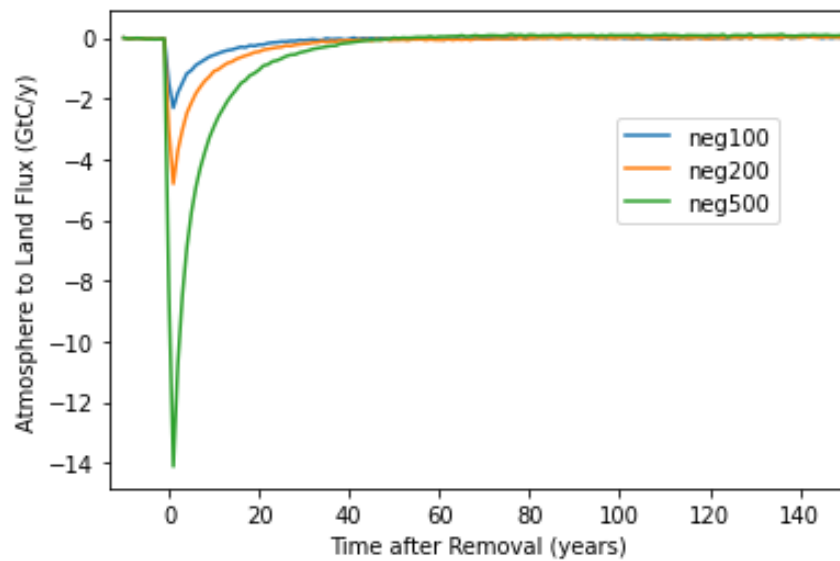# Appendix. Supplementary Figures and Tables

Figure A.1.:   Atmosphere to land flux for vs. time after removal (years) for CO_2 removals of -100GtC (blue), -200GtC (orange), and -500GtC (green) from the atmosphere. A negative flux indicates carbon is being released into the atmosphere.
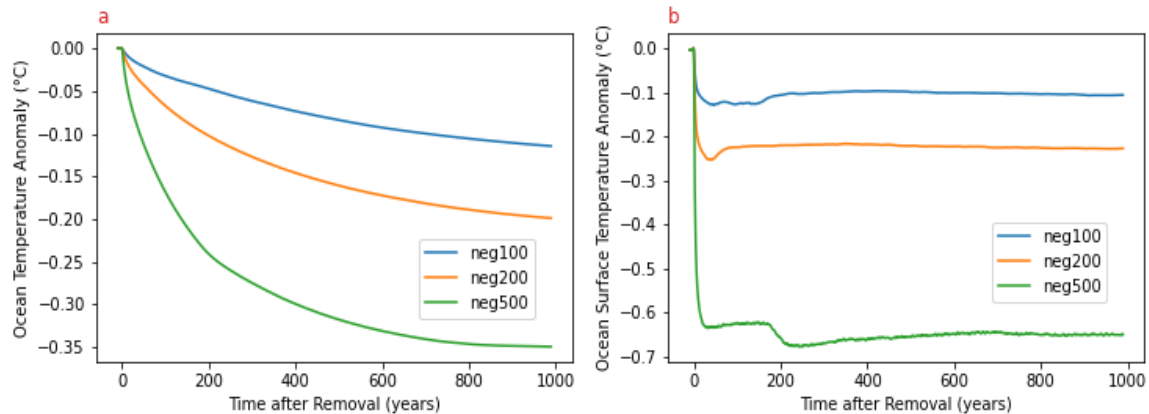

Figure A.2.:   Ocean temperature anomaly (a) and ocean surface temperature anomaly (b) vs. time after removal (years) for CO_2 removals of -100GtC (blue), -200GtC (orange), and -500GtC (green) from the atmosphere. Anomalies are calculated with respect to one year before the removal takes place.
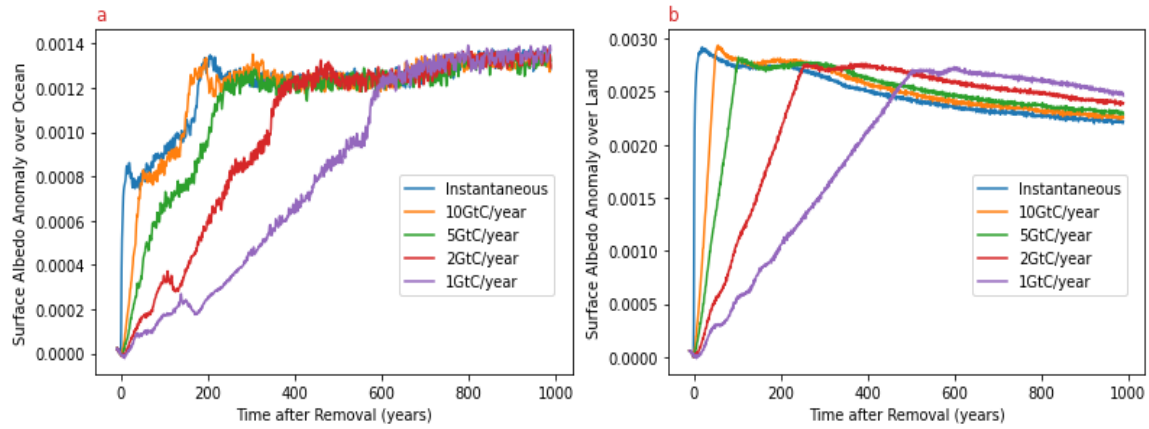
Figure A.3.:   Surface albedo anomaly over the ocean (a) and land (b) vs. time after removal (years) for all rates of removal in the neg500 removal scenario. Anomalies are calculated with respect to one year before the removal takes place.
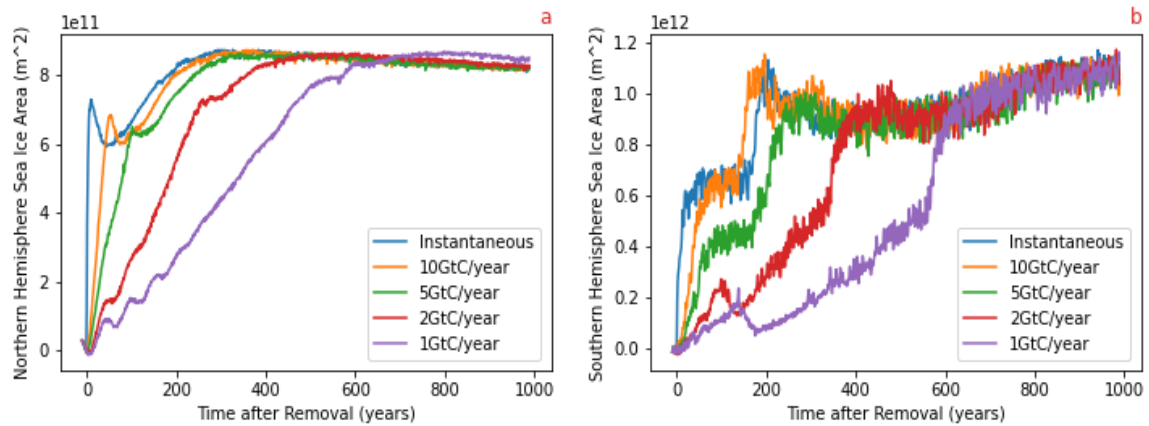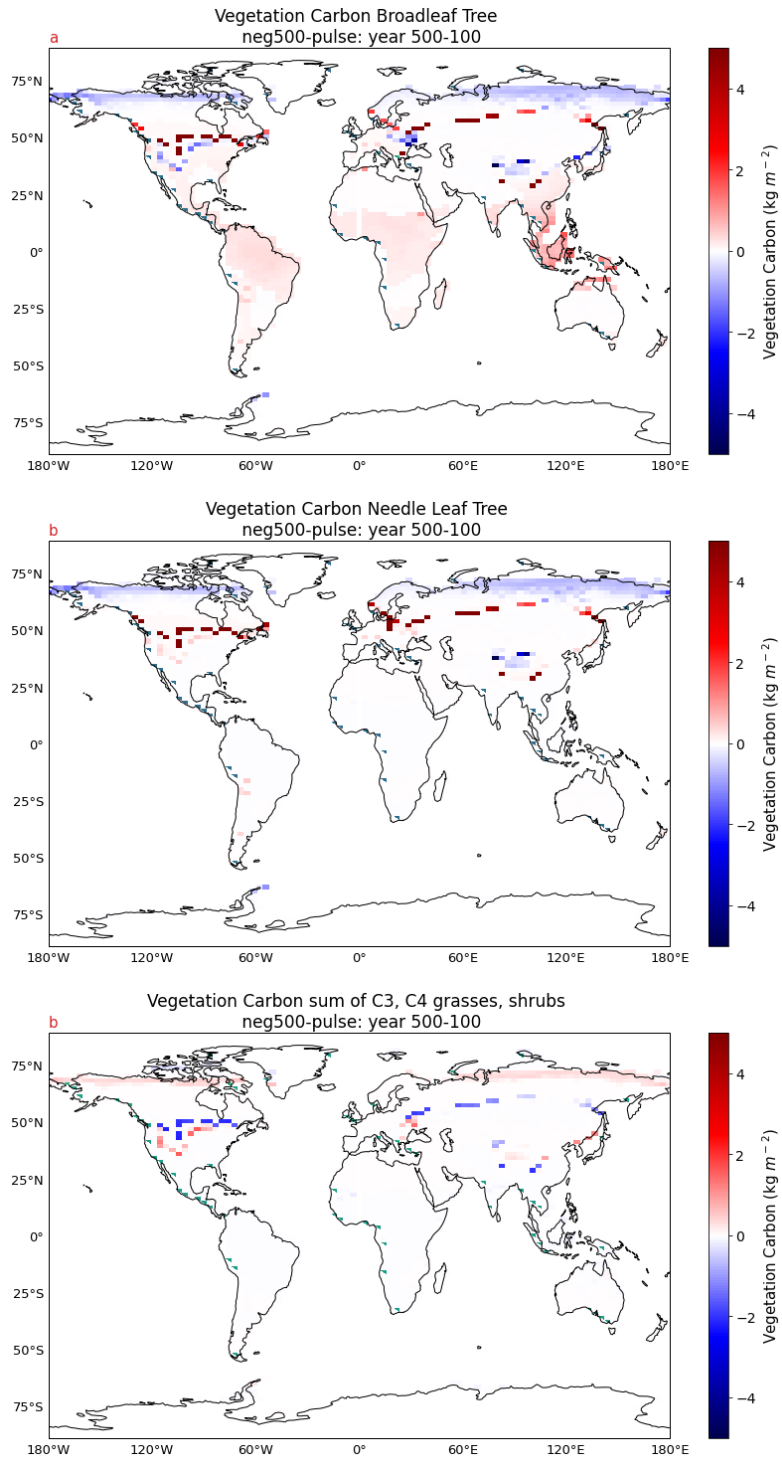

Figure A.4:   Northern Hemisphere sea ice area (a) and Southern Hemisphere sea ice area (b) vs. time after removal (years) for all rates of removal in the neg500 removal scenario. Anomalies are calculated with respect to one year before the removal takes place.

Figure A.5.: Vegetation carbon separated by broadleaf tree (a) needle leaf tree (b) and the sum of C3, C4 grasses and shrubs (c) for year 500-100 of the neg500 instantaneous rate simulation. C3, C4 grasses and shrubs show a similar and minimal change in vegetation carbon so they are grouped together in (c).
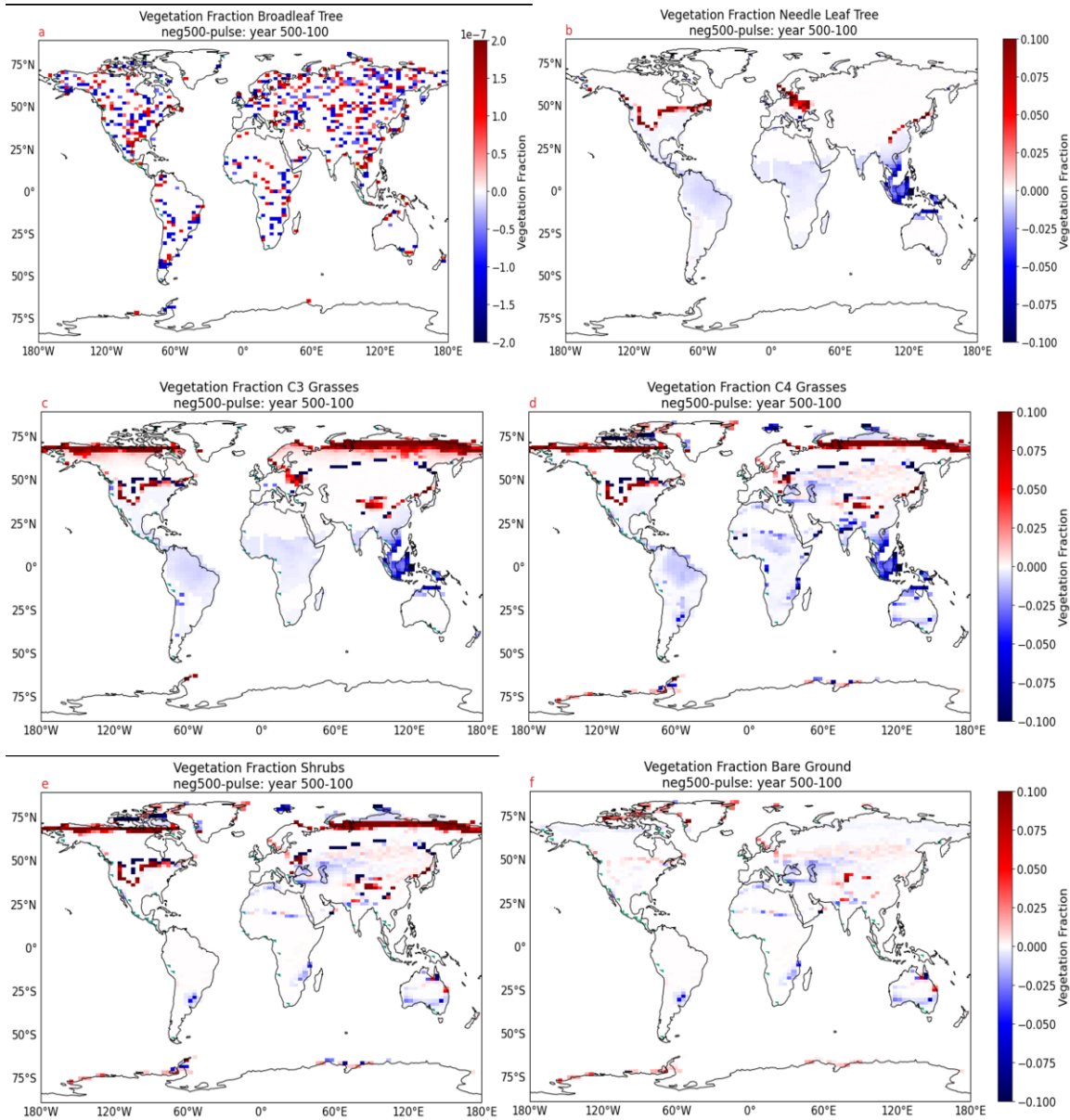
Figure A.6: Vegetation fraction broken down by PFT for year 500-100 of the neg500 instantaneous rate simulation. Changes in broadleaf trees are small and shown on a separate scale as its changes in fractional coverage are much smaller than the other PFTs.
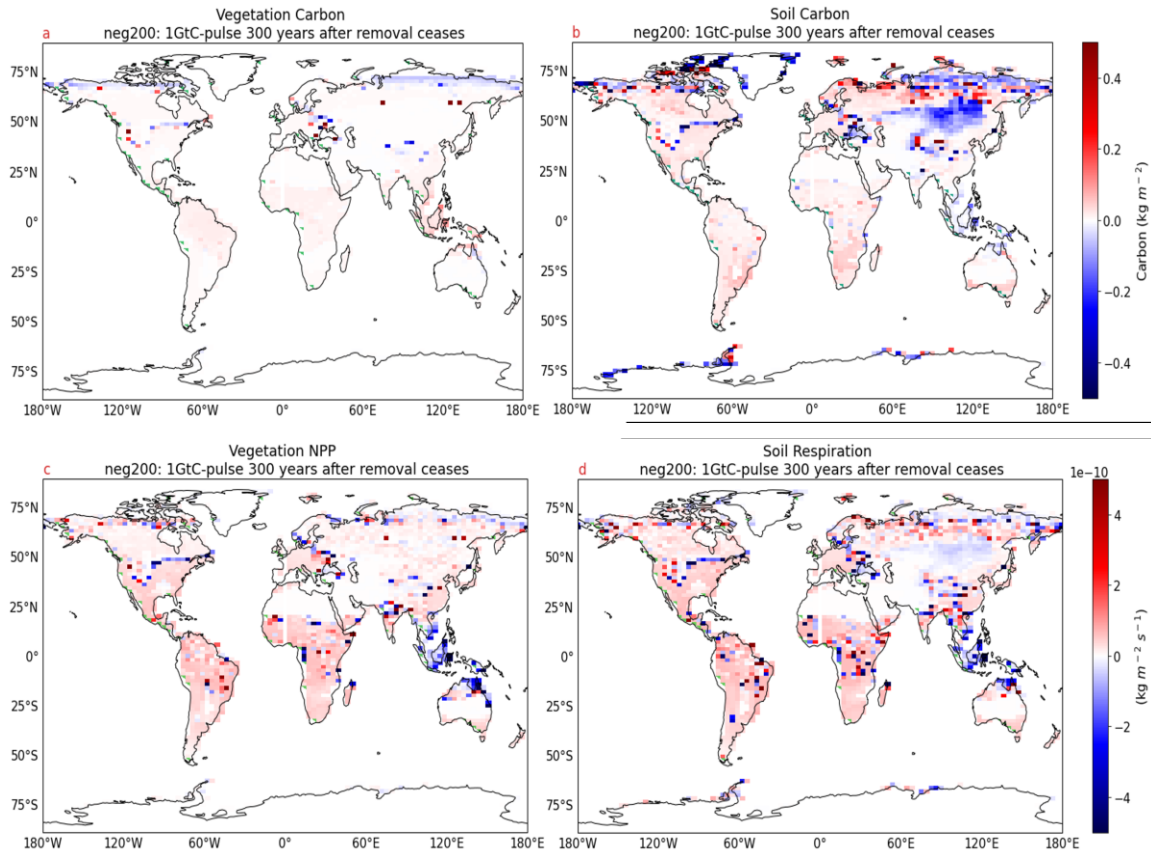
Figure A.7.: Vegetation carbon (a), soil carbon (b), NPP (c) and soil respiration (d) difference between the 1GtC and pulse removal rates for the 200GtC removal amount 300 years after the completion of the removal. Red areas are where the 1GtC rate shows greater values than the pulse, and the blue areas are where the 1GtC rate shows lesser values than the pulse. Figure shown to highlight the reduced differences between rates the further after removal is analyzed. Differences become less prominent 500 and 800 years after the completion of removal (not shown).
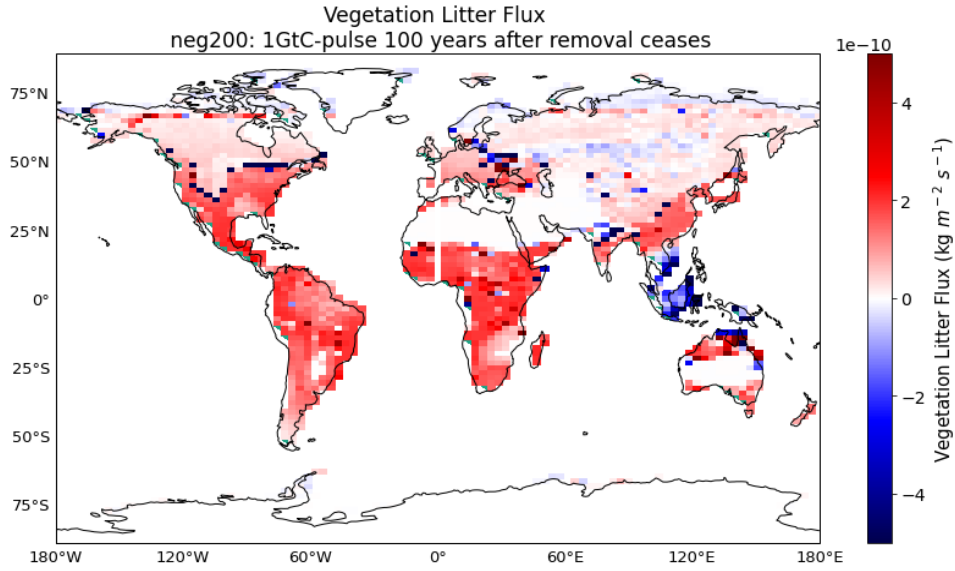
Figure A.8.   Vegetation litter flux for 1GtC-pulse rate in the neg200 removal amount scenario.
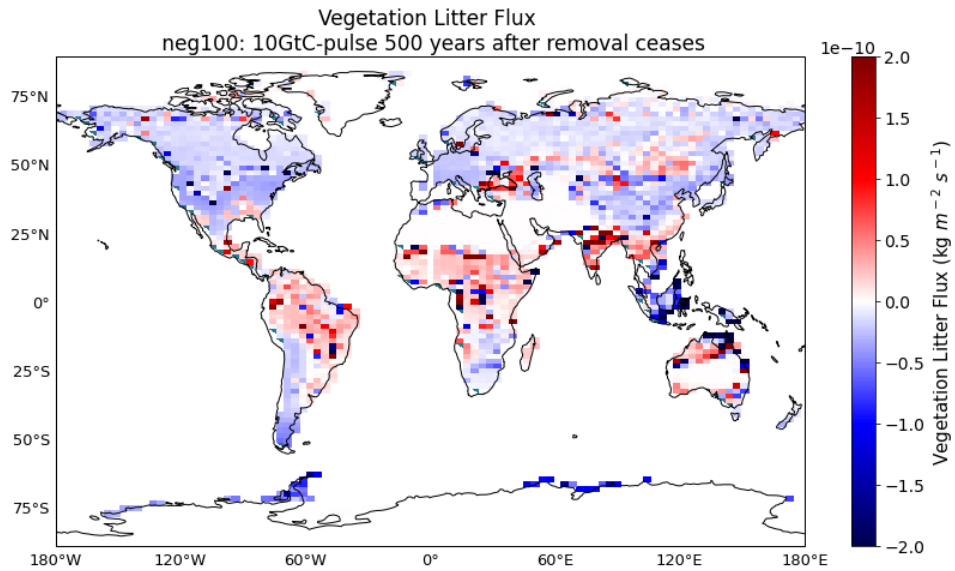

Figure A.9.:   Vegetation litter flux for 10GtC-pulse rate in the neg100 removal amount scenario.

Table A.1: Cumulative removal fraction for each rate within each amount. Calculations occur at 500 years following the completion of removal for each individual rate. At 500 years following the completion of removal the CRF does not depend much on the amount or rate of removal.

	100GtC	200GtC	500GtC
Instantaneous	0.37	0.37	0.38
10GtC/year	0.38	0.37	0.38
5GtC/year	0.37	0.37	0.37
2GtC/year	0.37	0.36	0.37
1GtC/year	0.37	0.36	0.36

Table A.2.: Cooling effectiveness for each rate within each amount. Units are °C/TtC. Calculations occur at 500 years following the completion of removal for each individual rate. The cooling effects of the neg100 10GtC simulation can be seen in this table by the increased effectiveness of that simulation in comparison to all other rates in the neg100 removal scenario.

	100GtC	200GtC	500GtC
Instantaneous	1.32 °C/TtC	1.48 °C/TtC	1.69 °C/TtC
10GtC/year	1.56 °C/TtC	1.47 °C/TtC	1.67 °C/TtC
5GtC/year	1.33 °C/TtC	1.46 °C/TtC	1.68 °C/TtC
2GtC/year	1.34 °C/TtC	1.46 °C/TtC	1.68 °C/TtC
1GtC/year	1.34 °C/TtC	1.46 °C/TtC	1.71 °C/TtC